

Self-reactive human CD4 T cell clones form unusual immunological synapses

David A. Schubert,¹ Susana Gordo,¹ Joseph J. Sabatino Jr.,³ Santosh Vardhana,^{4,5} Etienne Gagnon,¹ Dhruv K. Sethi,¹ Nilufer P. Sethi,¹ Kaushik Choudhuri,^{4,5} Helena Reijonen,⁶ Gerald T. Nepom,⁶ Brian D. Evavold,³ Michael L. Dustin,^{4,5} and Kai W. Wucherpfennig^{1,2}

¹Department of Cancer Immunology and AIDS, Dana-Farber Cancer Institute, and ²Program in Immunology, Harvard Medical School, Boston, MA 02215

³Department of Microbiology and Immunology, Emory University, Atlanta, GA 30322

⁴Program in Molecular Pathogenesis, Helen L. and Martin S. Kimmel Center for Biology and Medicine of the Skirball Institute of Biomolecular Medicine, and ⁵Department of Pathology, New York University School of Medicine, New York, NY 10016

⁶Benaroya Research Institute at Virginia Mason, Seattle, WA 98101

Recognition of self-peptide-MHC (pMHC) complexes by CD4 T cells plays an important role in the pathogenesis of many autoimmune diseases. We analyzed formation of immunological synapses (IS) in self-reactive T cell clones from patients with multiple sclerosis and type 1 diabetes. All self-reactive T cells contained a large number of phosphorylated T cell receptor (TCR) microclusters, indicative of active TCR signaling. However, they showed little or no visible pMHC accumulation or transport of TCR-pMHC complexes into a central supramolecular activation cluster (cSMAC). In contrast, influenza-specific T cells accumulated large quantities of pMHC complexes in microclusters and a cSMAC, even when presented with 100-fold lower pMHC densities. The self-reactive T cells also maintained a high degree of motility, again in sharp contrast to virus-specific T cells. 2D affinity measurements of three of these self-reactive T cell clones demonstrated a normal off-rate but a slow on-rate of TCR binding to pMHC. These unusual IS features may facilitate escape from negative selection by self-reactive T cells encountering very small amounts of self-antigen in the thymus. However, these same features may enable acquisition of effector functions by self-reactive T cells encountering large amounts of self-antigen in the target organ of the autoimmune disease.

CORRESPONDENCE

Kai W. Wucherpfennig:
kai_wucherpfennig@dfci.harvard.edu

Abbreviations used: cSMAC, central supramolecular activation cluster; GAD65, glutamic acid decarboxylase 65; HA, hemagglutinin; IRM, interference reflection microscopy; IS, immunological synapses; MBP, myelin basic protein; MCC, moth cytochrome c; MS, multiple sclerosis; pCD3ζ, phosphorylated CD3ζ; pMHC, peptide-MHC; pSLP-76, phosphorylated SLP-76; T1D, type 1 diabetes; TIRF, total internal reflection fluorescence.

MHC class II genes are strongly associated with susceptibility to several common human autoimmune diseases, including multiple sclerosis (MS) and type 1 diabetes (T1D; Todd et al., 1987; Hafler et al., 2007; Barrett et al., 2009). These genetic data imply that CD4 T cells specific for self-antigens play a central role in the pathogenesis of these diseases. Autoaggressive T cells need to escape negative selection despite self-antigen presentation in the thymus, yet also need to be able to respond to the self-antigen with sufficient strength in the target organ of the disease to initiate or sustain an autoimmune process. In some cases, escape from negative selection can be explained by absent or low-level presentation of the self-peptide in the thymus (Anderson et al., 2000; Klein et al.,

2000), but many self-antigens are in fact presented by medullary thymic epithelial cells (Derbinski et al., 2001; Anderson et al., 2002). Myelin basic protein (MBP) and glutamic acid decarboxylase 65 (GAD65) are well studied self-antigens that have been implicated in the autoimmune response in MS and T1D, respectively, and are both expressed in the thymus (Pribyl et al., 1996; Pugliese et al., 1997).

Crystal structures of self-reactive TCRs in complex with peptide-MHC (pMHC) have identified several unusual features within trimolecular complexes that may contribute to escape from negative selection. These structural alterations either affect the interaction of TCR

D.A. Schubert and S. Gordo contributed equally to this paper. N.P. Sethi's present address is Pfizer, Cambridge, MA 02139.

© 2012 Schubert et al. This article is distributed under the terms of an Attribution-Noncommercial-Share Alike-No Mirror Sites license for the first six months after the publication date (see <http://www.rupress.org/terms>). After six months it is available under a Creative Commons License (Attribution-Noncommercial-Share Alike 3.0 Unported license, as described at <http://creativecommons.org/licenses/by-nc-sa/3.0/>).

with pMHC or binding of self-peptide to the relevant MHC molecule. Three TCRs isolated from patients with MS were found to have unusual TCR binding modes. The Ob.1A12 and 3A6 TCRs, which recognized different epitopes of MBP, showed a shift of the TCR toward the peptide N terminus (Hahn et al., 2005; Li et al., 2005). The third TCR, Hy.1B11, bound with a highly tilted orientation which affected its interaction with both the MHC molecule and the MBP peptide (Sethi et al., 2011). Other mouse or human structures showed a conventional TCR orientation over the pMHC complex, but the interaction of the peptide with the respective MHC molecule was altered. The MBP_{Ac1-11} peptide (recognized by the mouse 172.10, 1934.4, and c19 TCRs) only partially filled the binding groove of I-A^u (He et al., 2002; Maynard et al., 2005; Feng et al., 2007). The MBP₁₁₄₋₁₂₆ peptide, recognized by the human MS2-3C8 TCR, bound with low affinity to HLA-DR4 as the result of a poor fit of the peptide into the binding groove (Yin et al., 2011). The seven structures determined so far have thus identified several distinct alterations of trimolecular TCR–pMHC complexes: altered TCR binding modes, partial filling of the peptide binding groove, or an impaired fit of the self-peptide in the groove.

What is the impact of such structural alterations on the formation of immunological synapses (IS) and early signaling events? TCR signaling is initiated in the IS, an elaborate and dynamic structure which forms at the interface of T cells and APCs (Monks et al., 1998; Grakoui et al., 1999). Imaging of synapse formation at high resolution on planar lipid bilayers with mobile pMHC complexes and ICAM-1 revealed that TCR signaling is initiated in microclusters that form primarily in the periphery of the interface. These microclusters typically contain phosphorylated TCRs, associated signaling molecules (such as ZAP-70 and SLP-76), and the CD28 co-stimulatory molecule (Campi et al., 2005; Yokosuka et al., 2005, 2008) but exclude the CD45 phosphatase (Johnson et al., 2000; Davis and van der Merwe, 2006). Microclusters are rapidly transported to the center of the synapse (central supramolecular activation cluster [cSMAC]) in an active transport process that requires actin polymerization (Varma et al., 2006; Kaizuka et al., 2007), ubiquitination of the TCR–CD3 complex, and the Tsg101 component of the ESCRT-1 complex (Vardhana et al., 2010). Signaling is sustained by continued formation of new microclusters in the periphery, which are then transported to the cSMAC, a site of TCR internalization (Yokosuka et al., 2005; Varma et al., 2006). In this study, we have examined how the organization of synapses formed by self-reactive T cells from patients with active autoimmune processes might differ from this well established paradigm for anti-microbial T cells.

RESULTS

Altered IS formation by a human T cell clone from an MS patient

Synapse formation can be imaged at high spatial and temporal resolution on glass-supported planar lipid bilayers

functionalized with mobile ICAM-1 and the appropriate pMHC complexes. All pMHC complexes were generated using DNP-labeled peptides and purified using an anti-DNP matrix as the final purification step to ensure homogeneous peptide loading. IS formation was first compared between the human self-reactive T cell clone Ob.1A12, isolated from a patient with relapsing–remitting MS, and the influenza hemagglutinin (HA)–specific T cell clone HA:D7. The Ob.1A12 T cell clone recognized the MBP₈₅₋₉₉ peptide presented by the MS-associated HLA-DR15 molecule (DRA, DRB1*15:01; previously termed DR2; Wucherpfennig et al., 1994), whereas HA:D7 T cells were specific for the influenza peptide HA₃₀₆₋₃₁₈ presented by HLA-DR4 (DRA, DRB1*04:01). As expected, the influenza-specific clone HA:D7 formed classical IS on lipid bilayers over a broad range of pMHC densities (1–100 pMHC/μm²; Fig. 1 A), similar to those previously reported for T cells with other specificities (Grakoui et al., 1999). These ISs were characterized by central accumulation of pMHC (cSMAC) from which ICAM-1 was excluded, as well as a surrounding area enriched in ICAM-1 (pSMAC). In striking contrast, no pMHC accumulation or cSMAC formation was detected when Ob.1A12 T cells were incubated on lipid bilayers that displayed low densities of pMHC (1–10 pMHC/μm²). Only when a high density of pMHC (100 pMHC/μm²) was used, minimal accumulation of pMHC was observed for some of the cells (<60% of the Ob.1A12 T cells). Despite this high pMHC density, cSMAC formation was observed only for very few cells (Fig. 1, B and D).

Synapse formation by both HA:D7 and Ob.1A12 T cells was followed at high pMHC densities (100 pMHC/μm²) over a time lapse of 90 min. The influenza-specific HA:D7 T cells stopped on the lipid bilayer shortly after application, accumulated ICAM-1, and formed pMHC microclusters (Campi et al., 2005; Yokosuka et al., 2005; Varma et al., 2006). These pMHC microclusters were then transported to the center of the synapse; within 15 min, >80% of cells formed mature cSMACs from which ICAM-1 was excluded by most of the cells. Once formed, the majority of these cSMACs were stable for the remainder of the observation period (Fig. 1 C and [Video 1](#)). In contrast, Ob.1A12 T cells showed limited pMHC accumulation, which ranged from small microclusters to larger patches (without cSMAC formation). pMHC accumulation was observed for ~40–60% of the cells, whereas cSMACs were formed by only 5% of the cells (Fig. 1 D and [Video 2](#)). No visible pMHC accumulation was observed when HA:D7 or Ob.1A12 T cells were incubated on lipid bilayers displaying control pMHC and ICAM-1 (Fig. 1 E).

Transgenic mice that express the Ob.1A12 TCR and HLA-DR15 develop severe experimental autoimmune encephalomyelitis spontaneously or after immunization with MBP peptide (Madsen et al., 1999; Ellmerich et al., 2005). T cells from these mice were tested for synapse formation to exclude the possibility that the observed phenotype was a result of long-term culture of the human T cell clone. T cell

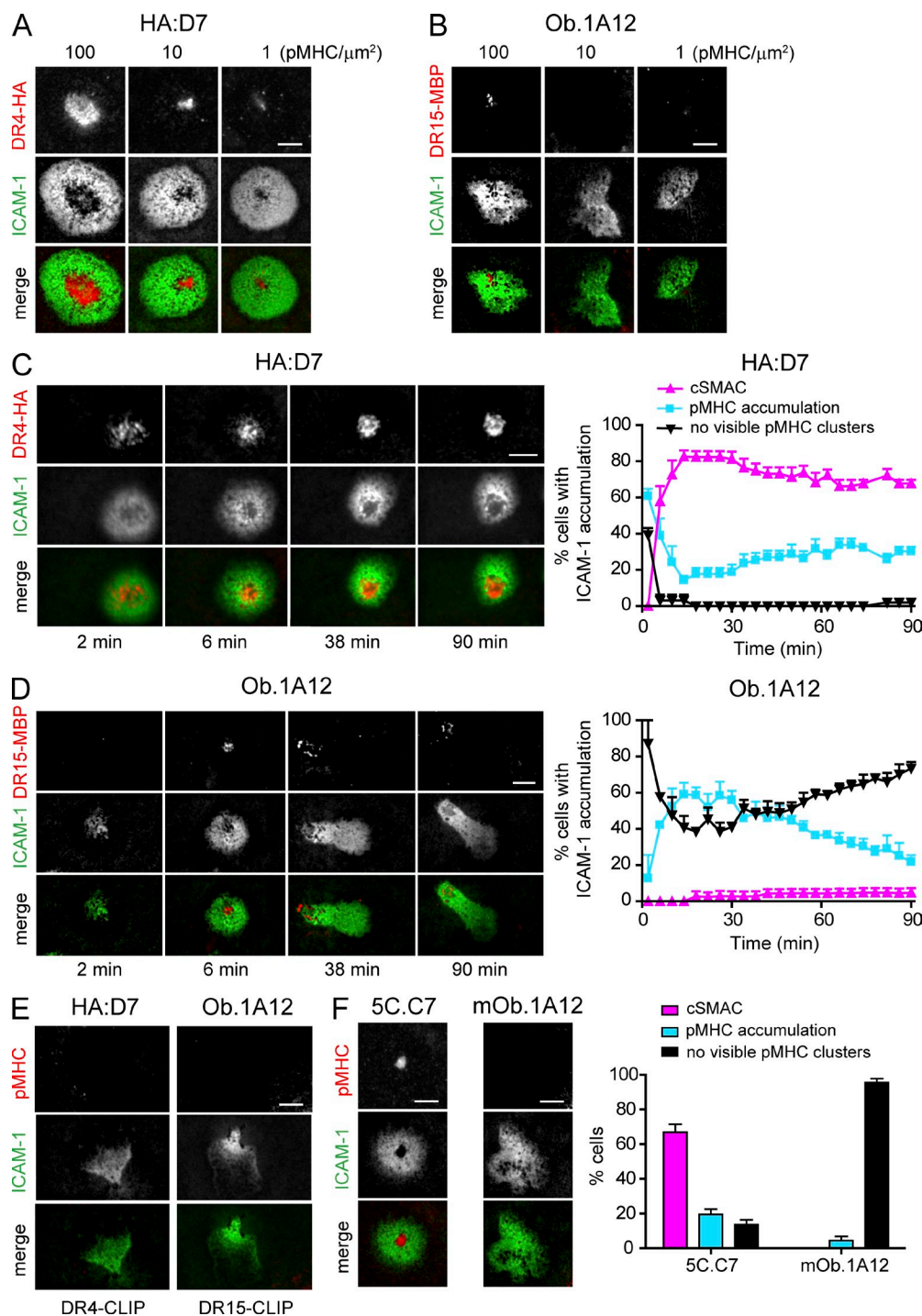


Figure 1. Altered synapse formation of self-reactive Ob.1A12 T cells on planar lipid bilayers displaying pMHC and ICAM-1. (A and B) Titration of pMHC complexes. HA:D7 and Ob.1A12 T cells were incubated on glass-supported planar lipid bilayers displaying ICAM-1 (~ 200 molec/ μm^2) and pMHC (DR4-HA or DR15-MBP) at ~ 1 , 10, and 100 molec/ μm^2 . Representative images at 30 min are shown. (C and D) Kinetics of IS formation by HA:D7 and Ob.1A12 T cells incubated on planar lipid bilayers containing pMHC (~ 100 molec/ μm^2) and ICAM-1. Each cell with ICAM-1 accumulation was categorized as showing cSMAC formation, pMHC accumulation without cSMAC formation, or no visible pMHC clusters. Graphs show mean percentage \pm SEM for three to four fields with 48–65 individual cells analyzed. (E) Specificity of pMHC accumulation. HA:D7 or Ob.1A12 T cells were incubated on lipid bilayers displaying control pMHC (DR4-CLIP or DR15-CLIP at ~ 100 molec/ μm^2) and ICAM-1. CLIP (class II-associated invariant chain peptide) was used as a control peptide. Images of ICAM-1 and pMHC at 30 min are shown. (F) Mouse 5C.C7 and mOb.1A12 T cell blasts were incubated on lipid bilayers displaying pMHC (~ 100 molec/ μm^2) and ICAM-1. Representative images at 30 min are shown. T cells with ICAM-1 accumulation were categorized as in C and D. Bar graph shows mean percentage \pm SEM for 7–11 fields with 130–161 individual cells analyzed. Data are representative of at least two experiments. Bars, 5 μm .

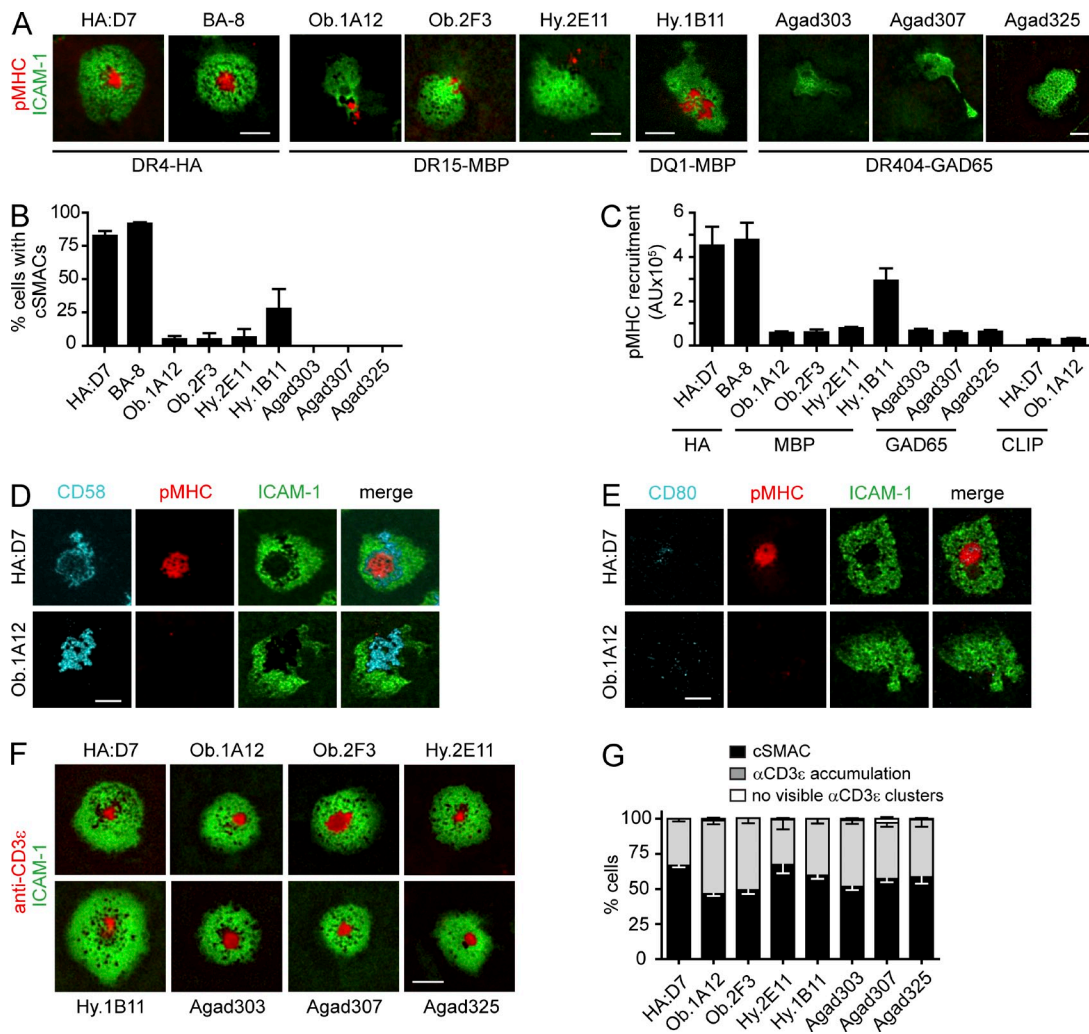


Figure 2. Impaired cSMAC formation and pMHC recruitment by self-reactive T cells on planar lipid bilayers. (A) Representative images for HA-specific clones (HA:D7 and BA-8), MBP-specific clones (Ob.1A12, Ob.2F3, Hy.2E11, and Hy.1B11), and GAD65-specific clones (Agad303, Agad307, and Agad325) on lipid bilayers displaying ICAM-1 and pMHC. Images were selected from a 20–90-min time period. (B) Quantification of cSMAC formation. The percentage of cells with ICAM-1 accumulation that formed a cSMAC was determined. Mean of at least three different fields \pm SEM over 90 min is shown. (C) Accumulation of pMHC at the interface. Integrated fluorescence of pMHC accumulation (in arbitrary units [AU]) was determined at 30 min for all cells that accumulated ICAM-1. Shown is the mean of 17–55 individual cells for each T cell clone \pm SEM. (D and E) Representative images of Ob.1A12 or HA:D7 T cells incubated on lipid bilayers displaying ICAM-1, pMHC, and CD58 or CD80 (~ 100 molec/ μm^2) at 30 min. (F and G) Representative images of T cells on lipid bilayers displaying anti-CD3 ϵ Fab fragment (~ 150 molec/ μm^2) and ICAM-1. T cells that accumulated ICAM-1 were categorized as follows: cSMAC formation, anti-CD3 ϵ accumulation, or no visible anti-CD3 ϵ clusters. Bar graph shows mean percentage \pm SEM for 4–13 fields with 80–319 individual cells analyzed. Data are representative of at least two experiments. Bars, 5 μm .

blasts from Ob.1A12 TCR transgenic mice were incubated on lipid bilayers displaying ICAM-1 and a high concentration of HLA-DR15-MBP₈₅₋₉₉ (~ 100 pMHC/ μm^2). Under these conditions, no cSMAC formation was observed and only minor pMHC accumulation was detected for very few cells (Fig. 1 F). However, mouse T cells that expressed the 5C.C7 TCR (specific for the moth cytochrome *c* [MCC] peptide [MCC₉₀₋₁₀₃] bound to I-E^k) formed classical IS when incubated on lipid bilayers with ICAM-1 and I-E^k-MCC at ~ 100 pMHC/ μm^2 (Fig. 1 F). These results showed that both human and mouse Ob.1A12 T cells had severe alterations in IS formation.

Limited pMHC accumulation and cSMAC formation by a panel of human self-reactive T cell clones

These results raised the question of whether the observed alterations in IS formation are also relevant for other self-reactive T cells. The study was extended to a panel of six additional T cell clones isolated from patients with two different autoimmune diseases, MS and T1D. Three T cell clones had been isolated from two relapsing-remitting MS patients and recognized the MBP₈₅₋₉₉ peptide either bound to HLA-DR15 (clones Ob.2F3 and Hy.2E11) or HLA-DQ1 (DQAI*01:02, DQBI*05:02; clone Hy.1B11; Wucherpfennig et al., 1994). The other three T cell clones originated from a T1D patient

and recognized the GAD65₅₅₅₋₅₆₇ peptide in the context of HLA-DR4 (DRA, DRB1*04:04; clones Agad303, Agad307, and Agad325; Reijonen et al., 2004). The GAD65₅₅₅₋₅₆₇ peptide represents a naturally processed epitope identified by peptide elution from purified HLA-DR4 molecules (Nepom et al., 2001). As a comparison to these self-reactive T cell clones, a second T cell clone specific for the influenza HA peptide HA₃₀₆₋₃₁₈ presented by HLA-DR4 (DRA, DRB1*04:01) was also included (clone BA-8).

The second influenza-specific clone (BA-8) formed classical IS with strong pMHC recruitment and cSMAC formation (Fig. 2, A–C). In contrast, little pMHC accumulation was observed in synapses formed by five of the six self-reactive T cell clones. Central accumulation of pMHC (cSMACs) was never observed for the three GAD65-specific T cell clones (Fig. 2 B and Video 3). Only few Agad303 and Agad325 T cells showed small pMHC clusters even when a previously characterized GAD65 analogue was used (557I; unpublished data). A small number of T cells from the MBP-specific clones Ob.1A12, Ob.2F3, and Hy.2E11 formed cSMACs (up to 6%, depending on the clone). Only Hy.1B11 T cells, specific for HLA-DQ1-MBP₈₅₋₉₉, showed a higher frequency of cSMAC formation (~25% of cells) and pMHC accumulation than the other six self-reactive clones (Fig. 2, B and C; and Video 4). For these six self-reactive clones, the total amount of pMHC recruited into the IS after 30 min was >5.8-fold lower compared with HA-specific T cells (Fig. 2 C). Addition of the co-stimulatory molecules CD80 and CD58 (ligands for CD28 and CD2) into the lipid bilayers had no impact on pMHC recruitment into synapses formed by MBP-specific Ob.1A12 T cells (Fig. 2, D and E). Recruitment of CD80 was low for all clones, probably as a result of low CD28 expression levels (unpublished data).

We also examined synapse formation with a fluorescently labeled, mono-biotinylated anti-CD3 ϵ Fab fragment and ICAM-1 anchored to lipid bilayers. Under these conditions, all self-reactive T cell clones and the antiviral clone HA:D7 showed strong accumulation of the anti-CD3 Fab fragment into the synapse, and 47–68% of the cells formed classical cSMACs. Only very few cells did not show anti-CD3 accumulation (Fig. 2, F and G). These results were important because they demonstrated that the unusual features of synapse formation were intrinsic to TCR interaction with self-pMHC complexes.

High motility of human self-reactive T cells

A second striking feature of self-reactive T cell clones was their continued motility on planar lipid bilayers. Most influenza-specific T cells stopped early after interacting with the lipid bilayer and remained stationary; some of these T cells started to migrate after some time. In contrast, most self-reactive T cells rarely came to a complete stop. The majority of cells migrated with variable velocities across the lipid bilayer, including even those cells for which some pMHC accumulation was visible (Fig. 3). Many migrating cells dragged accumulated pMHC behind the cell body, whereas ICAM-1 accumulated near the leading edge (Fig. 2 A and Videos 2 and 4). Interestingly, Hy.1B11 T cells migrated with high velocities across the lipid

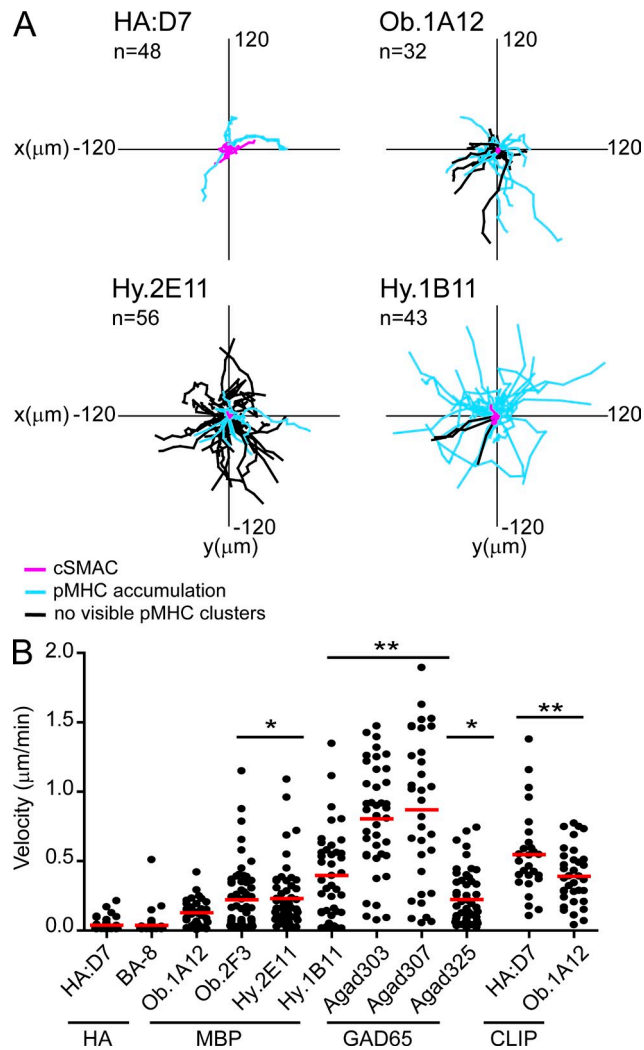


Figure 3. Continued motility of self-reactive T cells on planar lipid bilayers displaying pMHC and ICAM-1. Self-reactive and influenza-specific T cells were tracked for 90 min or for as long as they were present in the imaged field. (A) Tracks of T cell paths are shown. (B) Mean velocity of individual cells was quantified. Mean motility (indicated as red bars in B) of HA-specific T cell clones was compared with self-reactive T cell clones on lipid bilayers displaying appropriate pMHC, or HA:D7 and Ob.1A12 T cells incubated on lipid bilayers displaying control CLIP-MHC. Statistical analysis was performed using a one-way analysis of variance with Tukey's post test with * indicating $P < 0.05$ and ** indicating $P < 0.001$. For each T cell clone, 27–60 individual cells were analyzed. Each dot in the graph represents a single cell. Data are representative of at least two independent experiments.

bilayer despite accumulating pMHC into the synapse (Fig. 3, A and B). Only Agad303 and Agad307 T cells showed even higher velocities. These results showed that the self-reactive T cell clones not only formed abnormal synapses but also tended to maintain a striking degree of motility.

Impaired recruitment of TCR-CD3 complexes at T cell–B cell interface

Confocal imaging of T cell–B cell conjugates was performed to determine the relevance of these findings to T cell

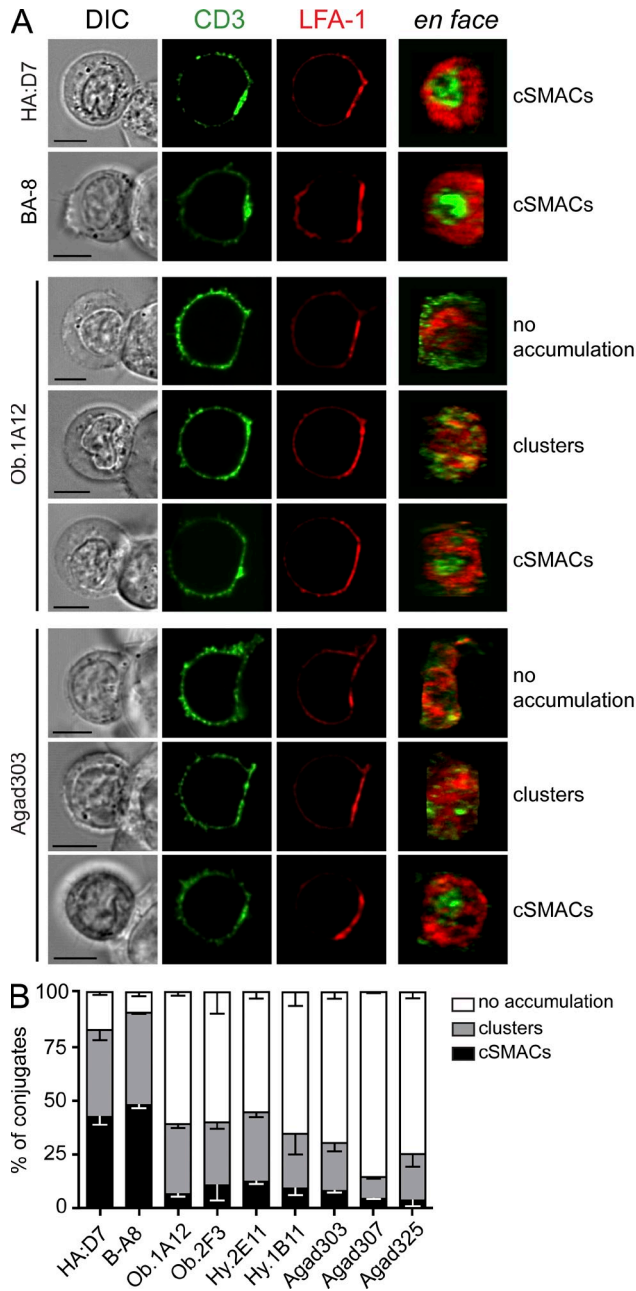


Figure 4. Impaired recruitment of TCR-CD3 complexes to synapses formed by self-reactive T cells and APC. (A) T cells were incubated for 30 min with peptide-pulsed EBV-transformed B cells and then fixed and stained for CD3 and LFA-1. Images on the right show an en face view of the contact area. Images for cells from HA:D7, BA-8, Ob.1A12, and Agad303 clones are shown to illustrate the different categories used for classification in B. Bars, 5 μ m. (B) Analysis of TCR-CD3 accumulation at the IS in self-reactive and HA-specific T cell clones. For each clone, 100–200 T cell–B cell conjugates were classified as cSMACs, TCR-CD3 clusters (not forming a mature cSMAC), or no TCR-CD3 accumulation. Bar graphs are shown with \pm SEM for two to three independent experiments.

interactions with live APC. T cells that formed an interface with a B cell (DIC image) and accumulated LFA-1 at the contact area were analyzed. Very few T cells formed conjugates

with B cells in the absence of the relevant peptide, indicating that peptide recognition is required for conjugate formation in this flow system (B cells attached to glass coverslip, injection of T cells). At least 40% of conjugates by the influenza-specific clones formed cSMACs, and an additional 35% showed strong recruitment of CD3 at the contact area in the form of clusters distributed over the interface (Fig. 4). In contrast, there was no visible accumulation of CD3 at the T cell–B cell interface for the majority of conjugates from all seven self-reactive T cell clones (55–85% of conjugates) when compared with the fluorescence of the T cell membrane outside of the contact area. This was also the case for the Hy.1B11 clone, possibly because HLA-DQ molecules are expressed at an \sim 10-fold lower level than HLA-DR molecules (Roucard et al., 1996). A small fraction of cells from all self-reactive clones formed cSMACs (<10% of conjugates). Some CD3 enrichment was observed at the interface of the remaining conjugates (10–30%), either as clusters of variable size or as an overall increase of fluorescence (with or without LFA-1 exclusion). Surface expression levels of CD3 on T cells or HLA-DR on B cells were comparable (unpublished data) and could not account for the observed differences in synapse formation. Thus, the findings described in the lipid bilayer system were relevant to the interaction of T cells with live APC.

Functional responses by self-reactive T cells

The limited recruitment of TCR to synapses formed by self-reactive T cells and peptide-pulsed B cells raised the question whether these T cells had substantial functional defects. The two HA-specific T cell clones proliferated in response to low doses of peptide ($EC_{50} \sim 0.15$ nM) and produced substantial quantities of IL-2 (Fig. 5, A and B). Surprisingly, MBP-specific Ob.1A12 and Ob.2F3 clones proliferated at \sim 100-fold lower peptide concentrations ($EC_{50} \sim 1.5$ – 1.2 pM) than the influenza-specific clones. Higher peptide concentrations were required for the five remaining self-reactive clones, in particular clones Agad307 and Agad325 ($EC_{50} \sim 65$ – 214 nM; Fig. 5 A). All self-reactive T cell clones also produced significant quantities of IL-2 (Fig. 5 B).

CD3 down-regulation and CD69 up-regulation were also evaluated for T cell–B cell conjugates (Fig. 5, C and D). Surface CD3 levels were substantially down-regulated within 2 h after activation for both HA-specific and self-reactive T cells. CD69, an early activation marker, was up-regulated by all clones. Negative regulators, such as PD-1 (surface) and CTLA-4 (intracellular), were expressed at later time points (unpublished data). The investigated self-reactive T cell clones thus mounted effector responses, despite the unusual features of synapse formation described in the previous sections.

Early signaling events in self-reactive T cells

These functional data prompted us to examine how early signaling events were initiated in self-reactive T cell clones. T cells applied to lipid bilayers were stained with an antibody directed against phosphorylated CD3 ζ (pCD3 ζ ; pY-142) as a readout of an early step in TCR signaling, the phosphorylation of CD3

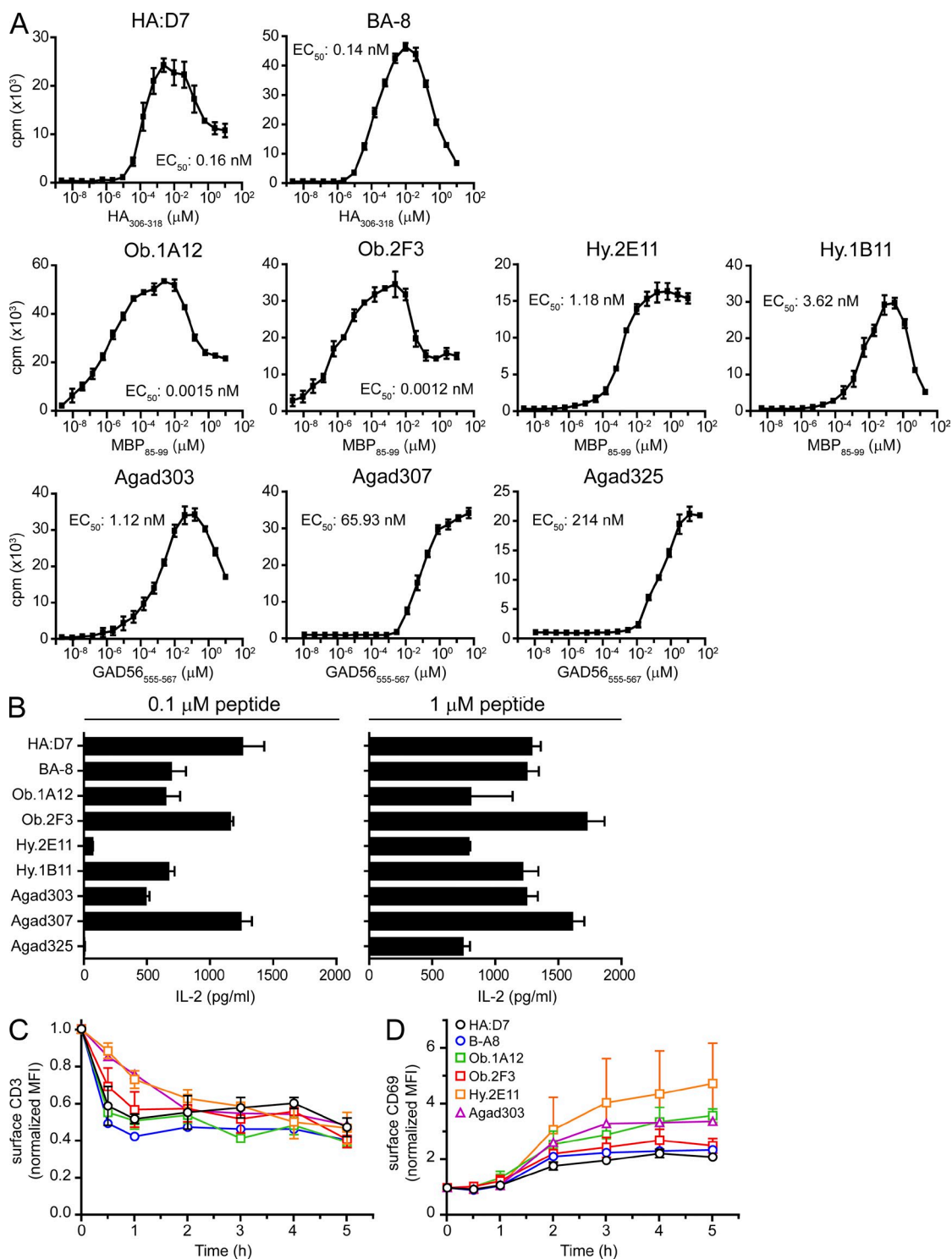


Figure 5. Self-reactive T cells respond to low peptide concentrations. (A) Proliferation of self-reactive and influenza-specific (HA:D7, BA-8) T cell clones. B cells were co-cultured with T cells for 72 h and peptides were added in serial dilutions in triplicates. Proliferation was measured by [3 H]-thymidine incorporation. Graphs show the mean \pm SD. Data are representative of at least two independent experiments. The peptide concentration required for half-maximal proliferation (EC_{50}) is indicated for each clone. (B) IL-2 secretion by self-reactive and influenza-specific T cells. T cells and B cells were co-cultured in the presence of 0.1 or 1 μ M peptide. After 24 h, supernatants were subjected to IL-2 quantification. Graphs show the mean \pm SD of triplicate measurements. Data are representative of at least two independent experiments. (C and D) TCR down-regulation and CD69 up-regulation on the cell surface. T cells were stimulated with peptide-pulsed B cells; at the indicated time points cells were stained with anti-CD3 and anti-CD69 antibodies and analyzed by FACS. MFI values were normalized to the MFI before stimulation. Graphs show the mean \pm SD of at least two independent experiments.

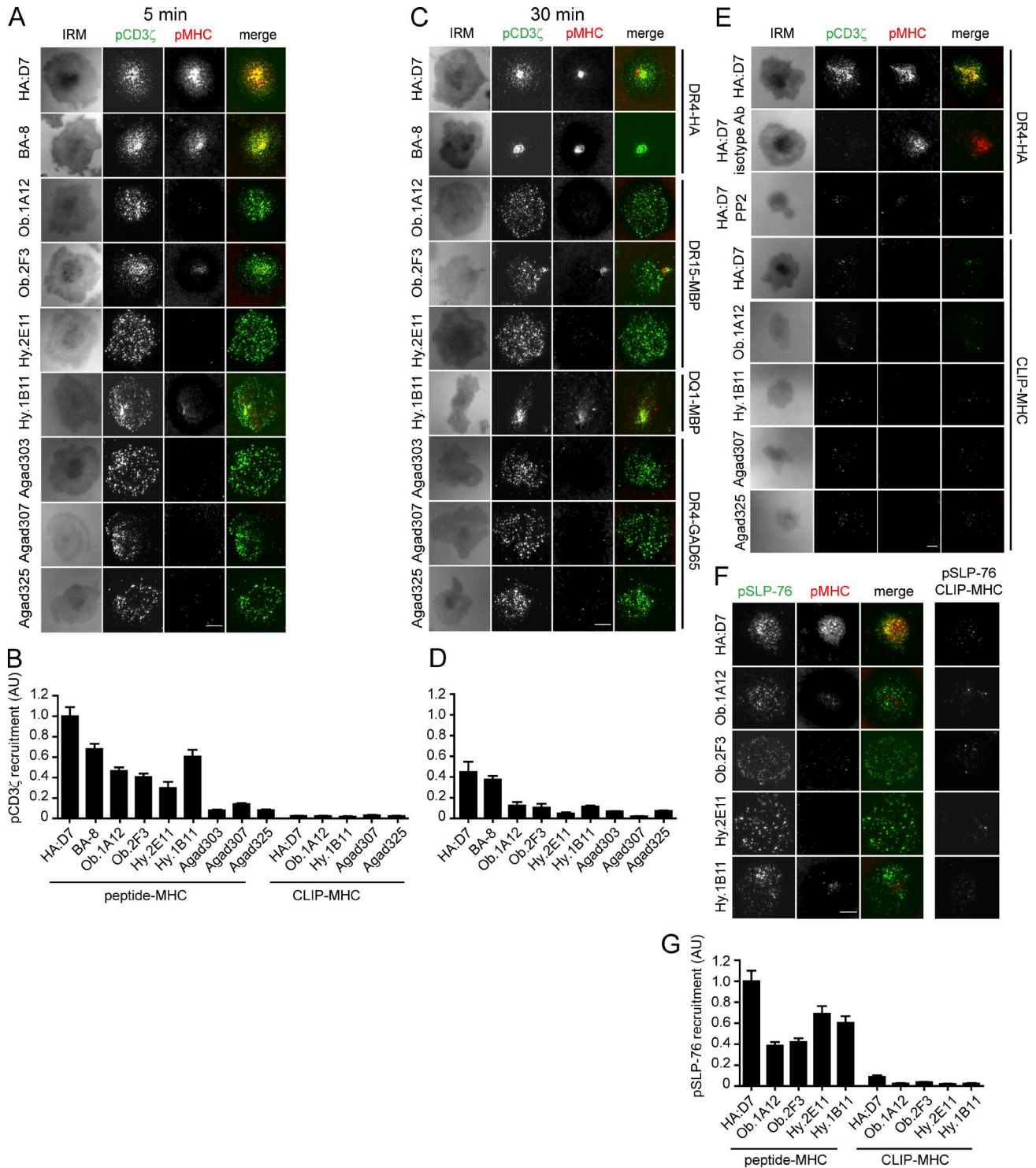


Figure 6. Self-reactive T cells accumulate phosphorylated TCR and SLP-76 into contact areas with the lipid bilayer despite little or no visible pMHC accumulation. T cells were incubated on lipid bilayers with ICAM-1 and pMHC. Cells were fixed after 5 or 30 min and stained for pCD3 ζ or pSLP-76. TIRF microscopy (TIRFM) was used to visualize pCD3 ζ or pSLP-76. (A–D) pCD3 ζ staining, pMHC fluorescence, and images for IRM are shown at 5 min (A) or 30 min (C). pCD3 ζ fluorescence at cell contact areas (defined by IRM images) at 5 min (B) or 30 min (D) was quantified and normalized to the value of HA:D7 fluorescence at 5 min. For each clone, 51–127 individual cells were analyzed. (E) Specificity of microcluster detection. Controls included: staining with isotype control antibody, treatment with Src kinase inhibitor PP2, and stimulation with irrelevant CLIP-MHC. Representative images at 5 min are shown. (F and G) pSLP-76 staining and pMHC accumulation at 5 min after stimulation with pMHC or CLIP-MHC. pSLP-76 fluorescence was quantified (G), as described in B. Data are representative of at least two independent experiments. Error bars in B, D and G represent the standard error of mean. Bars, 5 μ m.

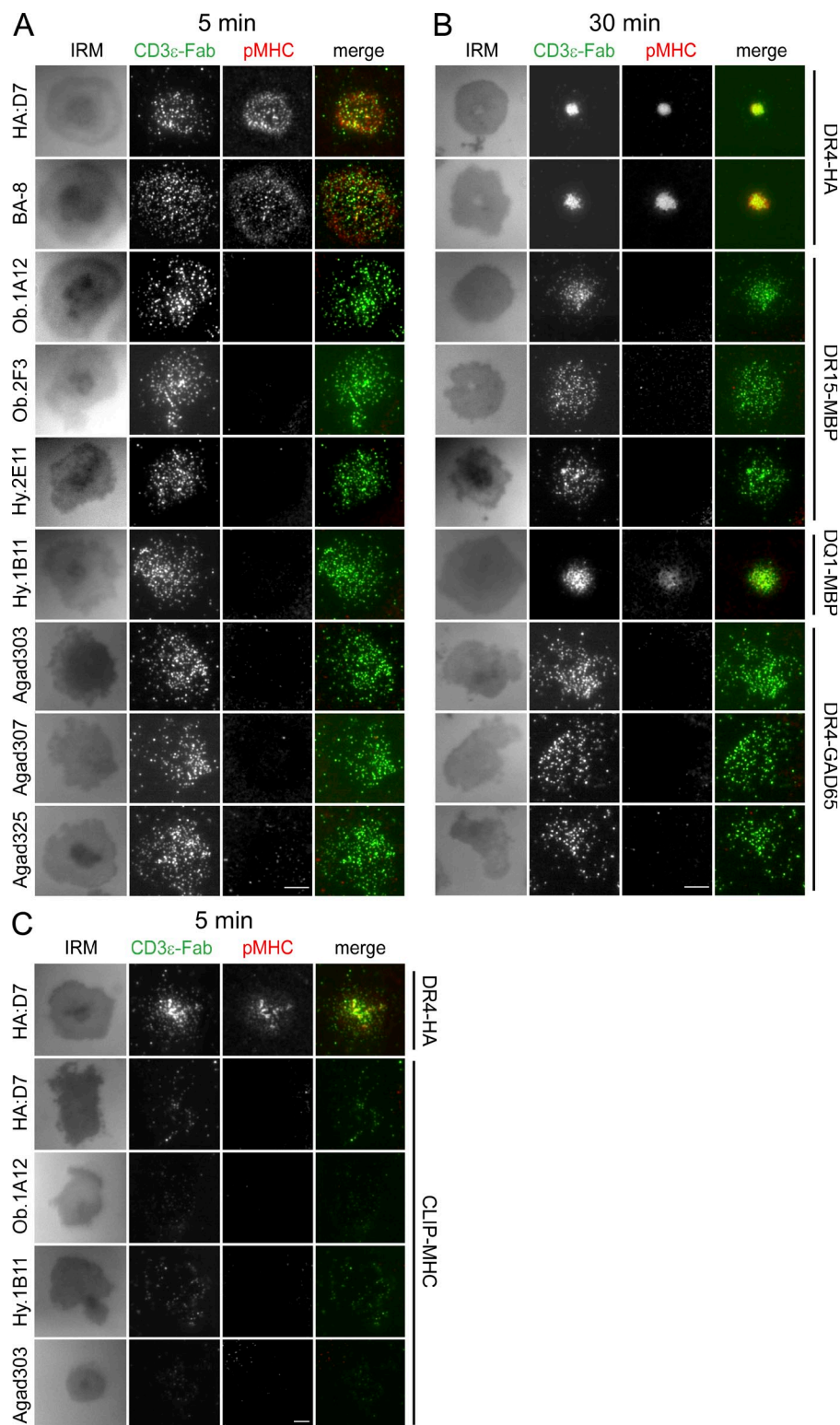


Figure 7. Detection of early TCR micro-cluster formation by self-reactive T cells with an anti-CD3 Fab fragment.

(A and B) T cells were stained with a fluorescently labeled Fab fragment specific for CD3 ϵ and then applied to lipid bilayers containing ICAM-1 and pMHC. Cells were fixed after 5 min (A) or 30 min (B) and IRM and fluorescence images for pMHC and CD3 ϵ were taken using TIRF microscopy. (C) Specificity of CD3 ϵ microcluster detection by stimulation with irrelevant CLIP-MHC. Representative images at 5 min are shown. Data are representative of at least two independent experiments. Bars, 5 μ m.

pCD3 ζ microclusters, even though very little or no pMHC accumulation was detectable (Fig. 6 A). Compared with HA:D7 T cells, the total amount of pCD3 ζ was 7.1–12.3 \times lower for the three GAD65-restricted T cells, and 2.1–3.4 \times lower for the three HLA-DR15 restricted MBP-specific T cells. Clone Hy.1B11 had the highest pCD3 ζ fluorescence among the self-reactive clones (Fig. 6 B). At 30 min, much smaller numbers of peripheral pCD3 ζ microclusters were observed for the HA-specific T cell clones, which had now formed cSMACs; pCD3 ζ fluorescence was still observed in these cSMACs. Peripheral pCD3 ζ microclusters were still present in most self-reactive T cells, indicative of ongoing signaling (Fig. 6 C), and again there was little or no visible pMHC accumulation except for clone Hy.1B11. Overall quantities of pCD3 ζ were lower for all clones at this later time point (Fig. 6 D).

Specificity of pCD3 ζ labeling was tested using several control conditions. No signal was detected in HA:D7 T cells that were applied to lipid bilayers and stained with an isotype control antibody. As an additional control, HA:D7 T cells were treated with a Src kinase inhibitor (PP2). PP2-treated cells interacted with the lipid bilayer but the contact area, as assessed on interference reflection microscopy (IRM) images, was greatly

reduced and only very few pCD3 ζ and pMHC microclusters were detected (Fig. 6 E). Only very few dim pCD3 ζ microclusters and no pMHC accumulation were detected when T cells from five different clones were incubated on lipid bilayers displaying control pMHC and ICAM-1 (Fig. 6, B and E).

reduced and only very few pCD3 ζ and pMHC microclusters were detected (Fig. 6 E). Only very few dim pCD3 ζ microclusters and no pMHC accumulation were detected when T cells from five different clones were incubated on lipid bilayers displaying control pMHC and ICAM-1 (Fig. 6, B and E).

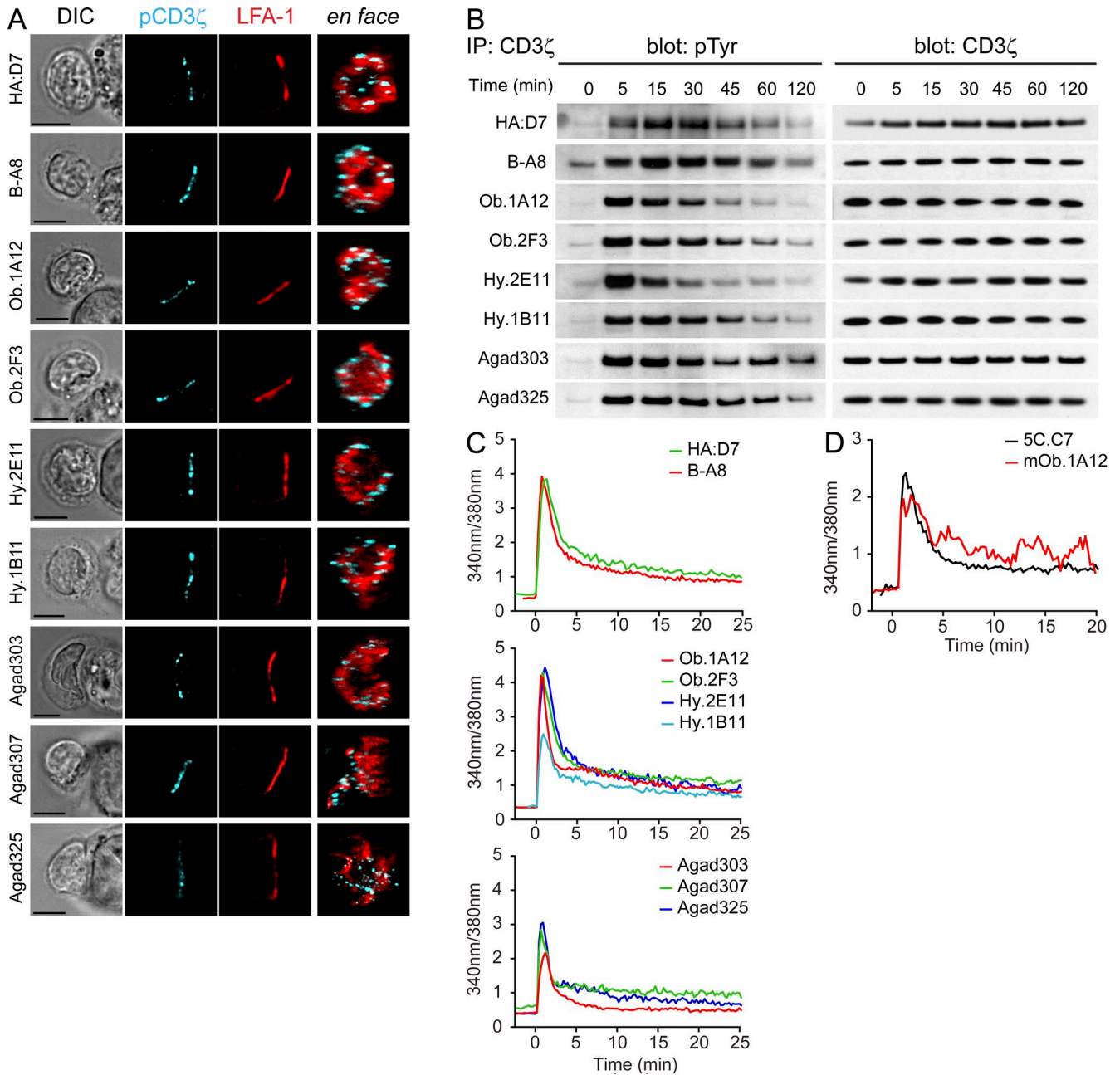


Figure 8. Early signaling events in self-reactive T cells with altered synapse formation. (A) Detection of microclusters of pCD3 ζ in T cells conjugated for 15 min with peptide-pulsed B cells. Images on the right show an en face view of the contact area. Bars, 5 μ m. (B) Kinetics of CD3 ζ phosphorylation upon antigen stimulation. T cells were stimulated with peptide-pulsed B cells; after stimulation, CD3 ζ was immunoprecipitated. Blots were probed for phosphorylated tyrosine (pTyr) and total CD3 ζ (loading control). (C) Calcium flux. Fura-2-labeled T cells were stimulated with peptide-loaded B cells. The profiles represent a mean of 20–45 individual cells, with time 0 being the initial contact of the T cell with the B cell. See [Videos 4–7](#) for examples. (D) Calcium mobilization in mouse 5C.C7 and mOb.1A12 TCR transgenic T cell blasts on lipid bilayers displaying ICAM-1 and pMHC. The profiles represent a mean of 33 individual cells, with time 0 being the initial contact with the lipid bilayer. Data are representative of at least two independent experiments.

Recruitment of the SLP-76 adaptor protein into the IS was observed within 5 min after addition of self-reactive T cells onto lipid bilayers (Fig. 6, F and G), indicating that later signaling events were also proceeding. Only minimal recruitment of phosphorylated SLP-76 (pSLP-76) microclusters was detected on lipid bilayers displaying control pMHC (Fig. 6, F and G).

When the TCR was labeled with a soluble fluorescent anti-CD3 ϵ Fab, TCR microclusters were detected after 5 and 30 min for most of the self-reactive T cell clones (Fig. 7, A and B), similar to the results obtained with the anti-pCD3 ζ antibody (Fig. 6, A and C). Lipid bilayers displaying control pMHC and ICAM-1 showed only few TCR microclusters

(Fig. 7 C). These data show that TCR microclusters can be readily detected for all tested self-reactive T cell clones, despite the alterations in synapse formation described in the previous sections.

Phosphorylation of CD3 ζ was also examined in T cell–B cell conjugates. Consistent with the data from the lipid bilayer experiments, microclusters containing pCD3 ζ were observed for all self-reactive T cell clones and they were primarily localized to the periphery of the contact area (Fig. 8 A). Brighter staining of pCD3 ζ microclusters was observed after 15 min of conjugate formation compared with a later time point (30 min), again in agreement with data from the lipid bilayer experiments. Interestingly, these microclusters were also detected in membrane extensions formed by some self-reactive T cells along the surface of B cells (Fig. 8 A, Agad307). TCR–CD3 phosphorylation was also examined by immunoprecipitation of CD3 ζ from T cell–B cell conjugates (Fig. 8 B). All clones showed strong CD3 ζ phosphorylation at early time points. CD3 ζ phosphorylation returned close to basal levels after 2 h, except for the GAD65-specific T cell clones. These results showed that phosphorylation of TCR microclusters proceeded in these self-reactive T cell clones despite little accumulation of self-pMHC complexes.

Signaling events subsequent to TCR phosphorylation

Mobilization of Ca²⁺ in T cells upon interaction with peptide-pulsed B cells was monitored using the Ca²⁺ indicator Fura-2 (Fig. 8 C). Despite the differences in synapse formation, the kinetics of early Ca²⁺ flux were similar among all self-reactive and HA-specific clones. No calcium flux was observed when B cells were not pulsed with the relevant peptide (unpublished data). Over 97% of all T cells showed a sharp increase of intracellular Ca²⁺ levels as soon as the T cell interacted with the B cell. Imaging of conjugate formation in real time confirmed that self-reactive T cells were more motile when interacting with APC than HA-specific clones (Videos 5–7). The motility of B cells and the three-dimensionality of the system prevented accurate quantification of this observation. There was no evident correlation between the individual Ca²⁺ profiles among motile versus stationary T cells. Similar kinetics of Ca²⁺ flux were also observed in freshly generated T cell blasts from TCR transgenic 5C.C7 and Ob.1A12 mice (Fig. 8 D) interacting with planar lipid bilayers, a finding which validates the use of the planar lipid bilayer system for the analysis of low-affinity self-reactive T cells.

Affinity and kinetics of TCR–pMHC binding

The two influenza-specific clones (HA:D7 and BA-8) were brightly stained by the appropriate tetramer (Fig. 9 A). However, there was little or no tetramer staining for six of the seven self-reactive T cell clones. Only Hy.1B11 T cells were stained by the relevant pMHC tetramer, which correlated with the finding that it was the only self-reactive clone with significant accumulation of pMHC in synapses formed on planar lipid bilayers.

Recently, new techniques have been developed that enable measurement of TCR binding kinetics in membrane

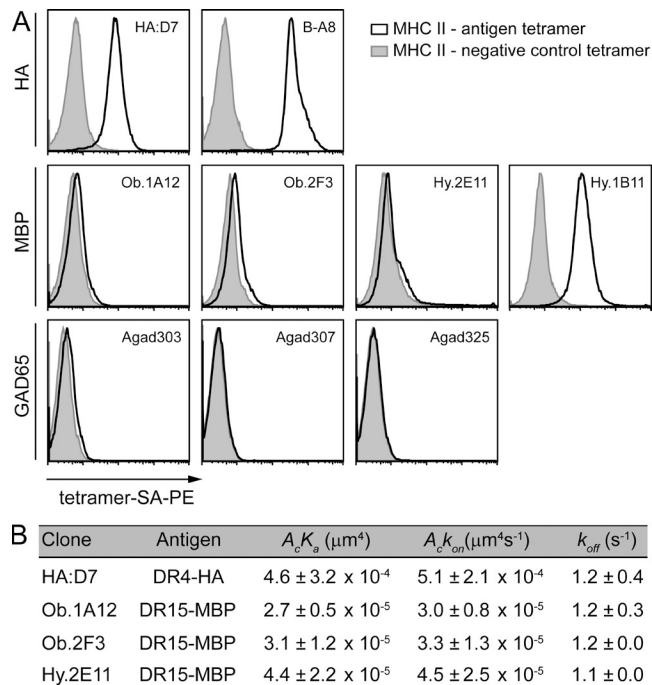


Figure 9. The majority of self-reactive clones have a low TCR

affinity for pMHC. (A). HA, MBP, or GAD65 reactive T cells were stained with control CLIP-MHC (MHCII-negative control tetramer) or the appropriate pMHC (MHCII-antigen tetramer) tetramers. (B) 2D affinities measured by the adhesion frequency micropipette assay for clones Ob.1A12, Ob.2F3, Hy.2E11, and HA:D7 (evaluated using the contact area [A_c]: $A_c K_{on}$ μm^4). The 2D off-rate (k_{off} s^{-1}) and the 2D on-rate ($A_c k_{on}$ $\mu\text{m}^4\text{s}^{-1}$) were also determined. Data are representative of at least two independent experiments.

interfaces (Huang et al., 2007, 2010; Huppa et al., 2010). The micropipette assay enables measurement of both low and high affinity interactions and is based on the initial interaction of T cells with RBCs coated with pMHC at defined densities (Fig. 9 B). T cells are micro-manipulated to touch the RBC with a controlled contact area and time. TCR–pMHC binding results in elongation of the RBC upon withdrawal, and this process is repeated many times to obtain an adhesion frequency from which kinetic rates related to the early binding process can be derived. Previous studies with the micropipette technique showed that TCR affinities could be measured for tetramer-negative T cell clones (Sabatino et al., 2011). We compared the binding kinetics and affinity for a tetramer-positive influenza-specific clone (HA:D7) and three tetramer-negative clones specific for MBP (Ob.1A12, Ob.2F3, and Hy.2E11). The three MBP-specific clones had similar affinities ($2.7\text{--}4.4 \times 10^{-5} \mu\text{m}^4$) which were ~ 10 -fold lower than for the HA-specific clone ($4.6 \times 10^{-4} \mu\text{m}^4$). Interestingly, the difference was not caused by the off-rate, which was very similar among all four clones ($1.1\text{--}1.2 \text{ s}^{-1}$). Rather, the on-rate was ~ 10 -fold slower for the three MBP-specific clones ($3.0\text{--}4.5 \times 10^{-5} \mu\text{m}^4\text{s}^{-1}$) compared with the influenza-specific clone HA:D7 ($5.1 \times 10^{-4} \mu\text{m}^4\text{s}^{-1}$). It thus appears that the alterations in synapse formation observed for these

Clone	HA:D7	BA-8	Hy.1B11	Ob.1A12	Ob.2F3	Hy.2E11	Agad303	Agad307	Agad325
Specificity	DR4-HA		DQ1-MBP	DR15-MBP			DR404-GAD65		
Disease	influenza		MS				T1D		
Tetramer staining	Orange	Red	Orange	Light yellow	Light yellow	Light yellow	Light yellow	Light yellow	Light yellow
cSMAC (lipid bilayers)	Red	Red	Yellow	Light yellow	Light yellow	Light yellow	Light yellow	Light yellow	Light yellow
CD3 recruitment (T-B conjugates)	Red	Red	Yellow	Light yellow	Light yellow	Light yellow	Light yellow	Light yellow	Light yellow
p-CD3 ζ recruitment (lipid bilayers)	Red	Orange	Orange	Light yellow	Light yellow	Light yellow	Light yellow	Light yellow	Light yellow
Motility	Red	Red	Yellow	Orange	Light yellow	Light yellow	Light yellow	Light yellow	Light yellow
Proliferation	Orange	Orange	Light yellow	Red	Red	Light yellow	Light yellow	Light yellow	Light yellow





	response	motility	proliferation
	80-100%	<0.1 $\mu\text{m}/\text{min}$	<0.005nM
	50-80%	<0.2 $\mu\text{m}/\text{min}$	<0.5nM
	10-50%	<0.5 $\mu\text{m}/\text{min}$	<5nM
	<10%	>0.5 $\mu\text{m}/\text{min}$	>50nM

Figure 10. Comparison of IS formation and signaling for a panel of seven self-reactive and two antiviral T cell clones. Parameters characterizing IS formation and signaling were compared using a color-coded grading system. Red indicates a response between 80 and 100% of the maximum response; orange, 50 and 80%; yellow, 20 and 50%; and light yellow, 0 and 10%. For motility, red represents <0.1 $\mu\text{m}/\text{min}$; orange, <0.2 $\mu\text{m}/\text{min}$; yellow, <0.5 $\mu\text{m}/\text{min}$; and light yellow, >0.5 $\mu\text{m}/\text{min}$. For proliferation, red corresponds to an EC_{50} <0.005 nM peptide; orange, <0.5 nM; yellow, <5 nM; and light yellow, >50 nM.

MBP-specific clones were caused by the slow on-rate (and resulting low affinity) of TCR binding to the DR15-MBP₈₅₋₉₉ complex.

DISCUSSION

Two main features characterize the altered synapses formed by the human self-reactive T cell clones examined here. First, central accumulation of TCR (cSMAC) was rarely observed, and recruitment of pMHC and TCR was low. Second, self-reactive T cells showed increased motility both on lipid bilayers and in T cell-B cell conjugates. In contrast, high affinity antiviral T cells were able to form classical IS even with a 100-fold lower density of pMHC on lipid bilayers. Nevertheless, early and late signaling events, as well as effector functions, could be induced in all self-reactive T cell clones over a wide range of peptide concentrations. All T cell clones formed mature synapses upon delivery of a strong activation signal with an anti-CD3 Fab fragment anchored to lipid bilayers, indicating that the unusual behavior of the self-reactive T cells was intrinsic to TCR recognition of self-pMHC complexes.

Despite these common features, we also observed substantial diversity among the MBP and GAD-specific T cell clones (Fig. 10). Overall, the MBP-specific clones showed more pMHC accumulation in synapses, greater quantities of pCD3 ζ in TCR microclusters at an early time point (5 min)

and proliferated at lower peptide concentrations than the GAD65-specific T cell clones. Motility was only slightly increased for Ob.1A12 T cells compared with the antiviral clones, but significantly higher for most other self-reactive clones, in particular Agad303 and Agad307 (which required higher peptide concentrations for activation). The minimal peptide concentration required for induction of T cell proliferation spanned a wide concentration range, with two MBP-specific clones (clones Ob.1A12 and Ob.2F3) responding even better than the two antiviral clones. Accumulation of pMHC and TCR was limited for all self-reactive clones except Hy.1B11 T cells; only the Hy.1B11 T cell clone was stained with the appropriate tetramer as the result of a higher pMHC affinity of the Hy.1B11 TCR (Sethi et al., 2011). Nevertheless, little pMHC-TCR accumulation was visualized for Hy.1B11 cells in T cell-B cell conjugates and relatively high peptide concentrations were required for activation in T cell proliferation assays. This can be explained by the lower surface expression of HLA-DQ compared with HLA-DR on APCs (Roucard et al., 1996). It thus appears that the higher TCR affinity of clone Hy.1B11 compensated for the low density of the relevant MHC class II molecule.

Previous studies showed that an altered peptide ligand (K99A) of MCC peptide recognized by the AND TCR could induce stronger T cell proliferation than the WT peptide

(Cemerski et al., 2007). The corresponding tetramer dissociated more rapidly than the WT tetramer, and cSMAC formation and TCR internalization were impaired for the K99A analogue (Cemerski et al., 2007; Vardhana et al., 2010). The human self-reactive T cell clones in our study were substantially different because they had considerably lower affinities (absence of tetramer staining for six of seven clones). Also, surface TCR internalization was observed for all self-reactive T cell clones with similar kinetics as for the HA-specific clones. Interestingly, a recent *in vivo* imaging study showed rapid, antigen-dependent TCR internalization that was not contingent on T cell motility arrest or cSMAC formation (Friedman et al., 2010).

The 2D measurements of TCR-pMHC binding with the micropipette system showed that three MBP-specific clones (Ob.1A12, Ob.2F3, and Hy.2E11) had an ~ 10 -fold lower affinity than a HA-specific clone (HA:D7). This lower affinity was the result of slower 2D on-rates for the MBP-specific TCRs, whereas the 2D off-rates were remarkably similar for all four tested clones. The slower 2D on-rates may be related to unusual structural features of TCR binding, as observed in the Ob.1A12 TCR structure (Hahn et al., 2005). Previous micropipette-based studies with the OT-1 T cell clone had shown that differences in 2D on-rate were dominant with respect to function (Huang et al., 2010). A recent study examined CNS-infiltrating CD4 T cells after induction of experimental autoimmune encephalomyelitis with the MOG₃₅₋₅₅ peptide. At the peak of clinical disease, eight times more CNS-infiltrating T cells specific for MOG were detected with the micropipette assay than by tetramer staining. Those lower affinity T cells also contributed significantly to cytokine production in the CNS (Sabatino et al., 2011). These data are consistent with our results documenting effector functions of low affinity self-reactive T cells and with the general observation that a large fraction of self-reactive T cells have a low affinity (tetramer-negative), yet some higher affinity self-reactive T cells (tetramer positive) are present.

How can low affinity binding of pMHC to TCR induce T cell activation? TCR microclusters are crucial signaling units for T cell activation; they form in the periphery of the contact area and migrate to the center during classical IS formation (Yokosuka et al., 2005; Varma et al., 2006). Recognition of low affinity self-antigen does not lead to massive TCR recruitment into the IS, yet is sufficient to induce early TCR-CD3 microcluster formation, phosphorylation, and eventually cytokine production and proliferation. TCR microcluster formation has even been reported for low affinity antagonist pMHC that induced incomplete CD3 ζ phosphorylation (Kersh et al., 1998; Grakoui et al., 1999; Sumen et al., 2004). Phosphorylated TCR microclusters formed by self-reactive T cells could be readily detected in the lipid bilayer system with an anti-CD3 ϵ Fab fragment or an antibody to the pCD3 ζ chain, but little pMHC was visualized in such microclusters. How can this striking result be explained? Recent work on TCR binding kinetics using the planar bilayer model showed that off-rates are ~ 10 -fold faster than

measured using biochemical techniques (Huppa et al., 2010). At the same time, adhesion molecules position pMHC and TCR on opposing membranes to greatly accelerate the on-rate. As a result of the fast off-rate, rapid rebinding of a few pMHCs by a larger number of TCRs in a microcluster (serial triggering) is likely to be essential to maintain signaling in a microcluster (Valitutti et al., 1995b; Huang et al., 2010; Huppa et al., 2010; Dustin and Depoil, 2011). The three MBP-specific T cell clones had a very similar off-rate as the studied antiviral clone, meaning that individual binding events lasted for a similar duration. Although small pMHC microclusters might have remained undetectable as a result of imaging limitations, our findings suggest that a substantial fraction of pMHC complexes diffused away after TCR microclusters had formed. Previous work showed that injection of an antibody which blocked the TCR-pMHC interaction did not disrupt established TCR microclusters but prevented formation of new microclusters (Varma et al., 2006). Thus, TCR microclusters formed by self-reactive T cells may have been stabilized by signaling complexes that linked individual TCRs, even though a substantial fraction of pMHC diffused away. A slow on-rate of binding is likely to disfavor effective T cell activation when very little antigen is present, as in the thymus for negative selection.

Upon recognition of antigen, signaling via TCR and integrins induces a stop signal that leads to rearrangements of the actomyosin cytoskeleton and restricts T cell motility (Grakoui et al., 1999; Samstag et al., 2003; Jacobelli et al., 2004). The signals that self-reactive T cells receive via their low affinity TCR may not be sufficient to achieve complete arrest. Ca²⁺-dependent phosphorylation of myosin IIA was reported to inhibit myosin-dependent motility (Jacobelli et al., 2004), but self-reactive T cells show increased motility despite Ca²⁺ mobilization, which may indicate a more complex mechanism. Nevertheless, TCR microcluster formation was shown to be independent of tyrosine kinase signaling (Campi et al., 2005) and was indeed intact in self-reactive T cells studied here. Sustained motility may allow these self-reactive T cells to continuously sample pMHC ligands so that signaling is maintained for sufficient lengths of time, despite reduced pMHC recruitment (Valitutti et al., 1995a). *In vivo* imaging studies have shown that T cells continue to crawl on dendritic cells that display cognate peptide during the early stages of a T cell response, which indicates that movement is compatible with TCR signaling (Mempel et al., 2004; Friedman et al., 2010). This mobile adhesive junction has been referred to as a kinapse (Dustin, 2007).

Our data show that signaling and effector functions can proceed for the self-reactive T cell clones studied here even when classical synapses are not formed. Prior work in the field has shown that organization of synapses is dependent on the type of APC, the quality of the presented antigen, the activation state of the T cell, and even the local environment in which the interaction takes place (Friedman et al., 2010). T cell blasts from TCR transgenic mice formed classical IS with peptide-pulsed B cells and on lipid bilayers, but thymocytes

from the same TCR transgenic mice did not show central accumulation of pMHC when they interacted with peptide-pulsed thymic epithelial cells or planar bilayers (Grakoui et al., 1999; Hailman et al., 2002; Richie et al., 2002). OT-II T cells showed central TCR-pMHC accumulation on planar lipid bilayers but formed multifocal synapses with dendritic cells (Tseng et al., 2008). Signaling could be observed long before spatial redistribution of receptors in the interface was complete (Lee et al., 2002) and naive T cells periodically break and reform synapses (Sims et al., 2007). The cSMAC has been identified as a site where TCR dephosphorylation takes place (Varma et al., 2006; Vardhana et al., 2010). Large numbers of pMHC complexes are sequestered in the cSMAC by high affinity TCRs, effectively removing them from the pMHC pool that can initiate formation of new microclusters. Reduced formation of cSMACs by the self-reactive T cell clones studied here may thereby reduce both TCR dephosphorylation and pMHC sequestration. Another study showed that the cSMAC may have an inhibitory function but can also be a site of sustained signaling depending on the time point and antigen quality (Cemerski et al., 2008). Interestingly, the antiviral T cell clones HA:D7 and BA-8 formed classical IS, but pCD3 ζ could still be detected in the cSMAC, which indicates that at least some signaling events were sustained in cSMACs formed by these cells under our experimental conditions.

How do self-reactive T cells fit into this functional diversity and what is the pathogenic potential of the studied T cell clones? Even though we analyzed seven human self-reactive T cell clones from patients with two different autoimmune diseases, these clones cannot fully represent the heterogeneity of self-reactive T cells present *in vivo*. The T cell clones were isolated from patients with active autoimmune processes and recognize self-antigens suspected to be key players in the pathogenesis. Nevertheless, the pathogenicity of human T cell clones is difficult to establish because passive transfer experiments would be unethical. Pathogenicity has been assessed for the Ob.1A12 TCR, and transgenic mice expressing the Ob.1A12 TCR and HLA-DR15 were found to develop spontaneous CNS inflammation and demyelination (Madsen et al., 1999; Ellmerich et al., 2005). Similar to the human T cell clones used in this study, Ob.1A12 transgenic T cells failed to form cSMACs or to accumulate visible pMHC into the IS even at high pMHC densities, showing that altered synapses can be observed in freshly generated T cell blasts from transgenic mice and are not merely a feature of long-term cultured human T cell clones. Despite impaired formation of IS, Ob.1A12 transgenic T cells mobilized Ca²⁺ on lipid bilayers displaying pMHC and ICAM-1, indicative of functional proximal signaling events. These data indicate that T cells with altered IS can have pathogenic potential.

Pathological self-reactive T cells need to escape negative selection in the thymus, despite thymic presentation of the self-antigen, such as MBP (Pribyl et al., 1996). Such escape may be facilitated by low affinity binding of a self-peptide to the relevant MHC molecule, low affinity TCR binding to pMHC, and/or low expression of the appropriate MHC

molecule (Wucherpfennig and Sethi, 2011). The impaired recruitment of pMHC complexes by these self-reactive T cells may have facilitated their escape from negative selection in the thymus. An important aspect is that most self-antigens are expressed in very small quantities by medullary thymic epithelial cells (Derbinski et al., 2001). In contrast, MBP is a highly abundant protein in the CNS myelin, and the presence of large quantities of this antigen is likely to facilitate the activation of MBP-specific T cells in the target organ of the disease, despite their impaired ability to form ISs.

MATERIALS AND METHODS

Reagents. Anti-CD3 ζ (pY142) (K25-407.69), anti-SLP-76 (pY128) (J141-668.36.58), and anti-human CD58 (1C3) were purchased from BD. Isotype antibodies mouse IgG2a, κ (MOPC-173) and mouse IgG1 κ (MOPC-21), anti-HLA-DR (L243), anti-human CD3 (UCHT1), anti-human CD4 (OKT4), anti-human CD11a/LFA-1 (HI111), anti-human CD54/ICAM-1 (MEM-111), anti-human CD69 (FN50), and anti-human CD80 (2D10) were obtained from BioLegend. Anti-human CD3 ζ (6B10.2) was purchased from Santa Cruz Biotechnology, Inc., anti-phospho-tyrosine (p-Tyr-100) from Cell Signaling Technology, and mouse IgG from Jackson Immuno-Research Laboratories. Anti-CD3 ϵ antibody (OKT3) was provided by the Dana-Farber Cancer Institute monoclonal antibody core facility; the OKT3 Fab fragment was generated using papain digestion, labeled with Alexa Fluor 647 (Invitrogen), and further purified using Protein G beads and gel filtration chromatography. The purified OKT3 Fab fragment did not induce Ca²⁺ flux in T cells. Monobiotinylated Fab fragments of CD3 ϵ -specific mouse mAb (UCHT1) were generated by pepsin digestion, followed by reduction with 0.5 mM 2-mercaptoethanol. Fab fragments were purified by FPLC, followed by supra-stoichiometric reaction with maleimide-derivatized biotin. Cy3 fluorophores were attached by amine coupling. Mono-biotinylation was confirmed by binding of Fab fragments to streptavidin-coupled beads and detection of other biotin moieties with an excess of fluorescently labeled streptavidin-allophycocyanin in solution (Fleire and Batista, 2009). This method was adapted from Brennan et al. (1985). Peptides were synthesized by Peptide 2.0 and JPT Peptide Technologies.

Mice. 5C.C7 T cell receptor transgenic mice on a RAG2^{-/-} B10.A background (Seder et al., 1992) were purchased from Taconic. Ob.1A12 TCR and HLA-DR15 (DRB1*15:01) transgenic mice on a C57/BL6 background were provided by D. Altmann (Imperial College, London, England, U.K; Ellmerich et al., 2005). All mice were housed under specific pathogen-free conditions and cared for in accordance with institutional and National Institutes of Health guidelines. Animal protocol was approved by the Institutional Animal Care and Use Committee at Dana-Farber Cancer Institute.

Cell culture. T cell clones HA:D7 and BA-8 were sorted from peripheral blood mononuclear cells from healthy donors using HLA-DR0401-HA₃₀₆₋₃₁₈ tetramers after *in vitro* expansion. Self-reactive T cell clones Ob.1A12, Ob.2F3, and Hy.2E11 (recognizing MBP₈₅₋₉₉-HLA-DR15 [DRB1*15:01]) and clone Hy.1B11 (recognizing MBP₈₅₋₉₉-HLA-DQ1 [DQAI*01:02, DQBI*05:02]) were previously isolated from patients with relapsing-remitting MS (Wucherpfennig et al., 1994). T cell clones Agad303, Agad307, and Agad325 (recognizing GAD₆₅₅₅₋₅₆₇-HLA-DR0404) were isolated from a T1D patient (Reijnen et al., 2004). Work with these blood samples had been approved by the institutional review boards of the Brigham and Women's Hospital and the Benaroya Research Institute. Human T cell clones were restimulated with PHA-L (Roche) in the presence of irradiated peripheral blood mononuclear cells and cultured in RPMI 1640 supplemented with 10% FBS, 2 mM GlutaMAX-I, 10 mM Hepes (all Invitrogen), 1% human serum (Valley Biochemical), and 5 U/ml rIL-2 (Roche), as previously described (Wucherpfennig et al., 1994). T cells were used between days 10 and 14 after restimulation.

Splenocytes from 5C.C7 and Ob.1A12 TCR transgenic mice were stimulated with 1 μ M MCC₉₀₋₁₀₃ or 2 μ M MBP peptide, respectively, in RPMI 1640 supplemented with 10% FBS, 2 mM GlutaMAX-I, 10 mM Hepes, 55 μ M 2-mercaptoethanol, 100 U/ml penicillin, and 100 μ g/ml streptomycin. On day 3 of culture, 30 U/ml hIL-2 was added and T cell blasts were used for experiments between days 7 and 8.

EBV-transformed B cell lines expressing the appropriate MHC class II molecules were used as APC in T cell–B cell conjugates and for proliferation and cytokine assays: MGAR (DRA, DRB1*15:01) for T cell clones Ob.1A12, Ob.2F3, Hy.2E11; 9009 (DQAI*01:02, DQBI*05:02) for T cell clone Hy.1B11; Priess (DRA, DRB1*04:01) for T cell clones HA:D7 and BA-8; and BLS0404 (DRA1*01:01, DRB1*04:04) and PE-117 (DRA1*01:01, DRB1*04:04) for T cell clones Agad303, Agad307, and Agad325. B cell lines were cultured in RPMI 1640 supplemented with 10% FBS, 2 mM GlutaMAX-I, and 10 mM Hepes.

Protein expression and purification. Soluble mouse ICAM-1 with a His₁₂-tag at the C terminus was produced from stably transfected Schneider cells (S2) and purified over an anti-ICAM-1 (YN1/1.7.4) affinity matrix followed by a Ni-NTA column (Dustin et al., 2007). ICAM-1 was labeled with Alexa Fluor 647 (Invitrogen) and subsequently purified using a Ni-NTA column.

All soluble MHC class II proteins were expressed with a covalently linked CLIP peptide attached to the N terminus of the β -chain via a thrombin-cleavable linker, and with a C-terminal BirA tag for site-specific biotinylation. Soluble HLA-DR0401 and HLA-DR15 molecules were expressed in stably transfected Chinese hamster ovary cell lines in hollow fiber bioreactors (Day et al., 2003). HLA-DQ1-CLIP was produced in glycosylation-deficient Lec3.2.8.1 cells (Stanley, 1989). HLA-DR0404-CLIP and I-E^K-CLIP (provided by M.M. Davis, Stanford University School of Medicine, Stanford, CA; Gütgemann et al., 1998) were produced in Sf9 *Spodoptera frugiperda* insect cells. HLA-DR molecules were purified using an anti-DR (L243) affinity matrix. HLA-DQ1 was purified using an anti-DQ/DR (9.3F10) column. I-E^K was expressed with a His-tag and was purified over a Ni-NTA column. Biotinylation was performed as previously described (Anders et al., 2011). CLIP peptide was cleaved with thrombin and peptide loading was performed overnight at 30°C in citrate-buffered saline, pH 5.2, in the presence of 1 mM EDTA, protease inhibitors, and the small molecule J10 that accelerates peptide loading (Nicholson et al., 2006). All peptides used in the loading reaction were synthesized with a DNP group on an introduced C-terminal lysine. pMHC complexes were finally purified using a Superose 12 gel filtration column (GE Healthcare) and an anti-DNP affinity matrix.

Soluble human CD58/LFA-3 (res. 29–215) and human CD80/B7-1 (res. 35–242) were expressed with an HA-tag at the N terminus and a His₁₀ tag at the C terminus in Sf9 insect cells and were purified by affinity chromatography using an anti-HA affinity matrix (Roche) followed by a Ni-NTA column (Invitrogen). CD58 was fluorescently labeled on the single free Cys166 with Alexa Fluor 488–C₅-maleimide (Invitrogen). CD80 was labeled with an Alexa Fluor 488 labeling kit (Invitrogen). Fluorescently labeled proteins were further purified using a Ni-NTA matrix.

Imaging on lipid bilayers. Glass-supported planar lipid bilayers were generated by applying DOPC liposomes containing 15% Ni-NTA-DGS and 0.05% cap-biotin-PE lipids (all Avanti Polar Lipids) on acid-cleaned coverslips that were placed into an FCS2 flow cell (Bioptechs). Flow cells were flushed with Hepes-buffered saline supplemented with 6 mM glucose, 2 mM MgCl₂, 1 mM CaCl₂, and 1% human serum albumin (SeraCare Life Sciences; HBS/HSA). Lipid bilayers were blocked with 5% casein in PBS containing 100 μ M NiCl₂. Polyhistidine-tagged ICAM-1 (~200 molec/ μ m²), CD58, and CD80 (~100 molec/ μ m²) were captured onto bilayers by binding to Ni-NTA-DGS lipids. Mono-biotinylated pMHC (~1–100 molec/ μ m²) was captured by Alexa Fluor 546-labeled streptavidin (Invitrogen), which was first applied to the bilayers. Monobiotinylated and Cy3-labeled anti-CD3 ϵ Fab fragment (UCHT1; ~150 molec/ μ m²) was captured by streptavidin (Thermo Fisher Scientific). Protein densities were determined by

staining the functionalized lipid bilayers with FITC-labeled antibodies and comparing the fluorescence under the microscope to FITC-labeled standard beads (Bangs Laboratories). T cells were cultured for 2–3 h in the absence of IL-2 before application to lipid bilayers. In some experiments, T cells were treated with the Src kinase inhibitor PP2 (100 μ M; EMD) for 1 h at 37°C in HBS/HSA buffer and then directly applied to the bilayers.

IS formation was followed on an inverted Nikon-TE microscope with perfect focus system and Prior Stage. At each time point, IRM, fluorescence, and brightfield images were taken through a 60 \times Plan-Apo VC DIC NA 1.4 oil objective using a 14-bit Clara Interline High-Resolution CCD Camera (Andor Technology). A Nikon Metal Halide was used as a light source and filter wheels were equipped with appropriate excitation and emission filters. For IRM images a custom-made filter set was used (470/40 nm excitation and 400 nm LP dichroic filter; Chroma Technology). Filter wheels and shutters (Sutter Instruments), stage, illumination and microscope were controlled using Andor iQ software. Experiments were performed at 37°C in a temperature-controlled environmental chamber.

Immunostaining of T cells on lipid bilayers and total internal reflection fluorescence (TIRF) microscopy. For visualization of recruitment of pCD3 ζ or pSLP-76 into the IS, T cells were applied to lipid bilayers and fixed at the indicated time points with 2% formaldehyde for 20 min. Cells were permeabilized with 0.1% NP-40 in HBS/HSA, blocked with 5% casein in PBS, and stained with Alexa Fluor 488-labeled antibodies for 20 min. For visualization of CD3 microclusters, T cells were first labeled with 20 μ g/ml fluorescently labeled OKT3-Fab fragment for 20 min at 37°C and then directly injected onto the bilayers; cells were fixed at the indicated time points.

TIRF microscopy imaging was performed on an inverted microscope (Ti-E; Nikon) equipped with motorized control of a TIRF laser illumination unit. All TIRF images were acquired through a 100 \times Apo TIRF NA 1.49 oil objective. TIRF imaging was done with excitation from solid state lasers delivered via a single optical fiber into the TIRF arm (Andor) and quad TIRF filter set with single pass emission filters in an emission filter wheel. TIRF angle alignment was performed according to the manufacturer's instructions.

T cell-APC conjugates for confocal microscopy. EBV-transformed B cells were pulsed with 1 μ M peptide for 3 h, washed, resuspended in Ringer's solution, and immobilized on an acid-cleaned coverslip in a laminar flow chamber FC2 (Bioptechs). T cells were then injected (in RPMI 1640 media) and allowed to interact with the B cells for 15 or 30 min at 37°C. Conjugates were fixed with 1% formaldehyde in PBS for 15 min at room temperature, blocked in 3% FBS, and stained with antibodies for extracellular receptors (Alexa Fluor 488 anti-CD3 and/or Alexa Fluor 647 anti-LFA-1). For detection of pCD3 ζ , cells were briefly fixed after extracellular staining, permeabilized with 0.05% Triton X-100 in PBS, blocked in 5% casein/50 μ g/ml mouse IgG in PBS, and stained with Alexa Fluor 488 anti-CD3 ζ (pY142) for 30 min.

Imaging was performed in a laser-scanning confocal microscope (SP5X; Leica) equipped with Acousto Optical Beam Splitter (AOBS) system and motorized x-y-z stage. Fluorophores were simultaneously excited with an Argon laser (488 nm) and a white light laser (647 nm). Specific fluorescence emission wavelengths were detected with photomultiplier tubes through adjusted spectral windows. Images were acquired through a 63 \times Plan Apo oil NA 1.4 objective with 1 μ m pinhole, at 256 \times 256 bytes resolution, 700 Hz scanning rate, and line averaging and accumulation of 2. Z stacks were collected at 0.15–0.2- μ m steps.

Image analysis and statistical analysis. All images were processed and analyzed using Andor IQ software (Andor Technology) or Image J software (National Institutes of Health). Statistical analysis was performed using Prism (GraphPad Software).

Ca²⁺ flux microscopy. T cells were loaded with Fura-2 (Invitrogen) and injected into flow chambers containing peptide-pulsed B cells or lipid bilayers. Imaging was performed on an inverted Nikon-TE microscope through a 20 \times S Fluor NA 0.75 air objective. Fura-2 was excited in 15 s (for T cell–B cell conjugates) or 20 s (on lipid bilayers) intervals using a Lambda DG-4

unit (Sutter) with 340 and 380 nm excitation filters. Emission was captured through a 510 ± 40 nm bandpass filter (Semrock) by a 14-bit Clara Interline High-Resolution CCD Camera (Andor Technology). After 1 h, $1 \mu\text{M}$ ionomycin was injected as a positive control.

Immunoblotting. EBV-transformed B cells were pulsed with $0.2 \mu\text{M}$ peptide for 3 h. T cells were cultured in the absence of IL-2 for 3 h (to minimize basal phosphorylation) and treated with $20 \mu\text{g}/\text{ml}$ cycloheximide (Sigma-Aldrich) for 1 h before the experiment. T cells and B cells were mixed at a 3:2 ratio (8×10^6 T cells per time point), briefly spun down, and incubated at 37°C . Upon stimulation, pelleted cells were flash frozen and lysed at 4°C in freshly made lysis buffer: 1% vol/vol NP-40 (US Biological), 20 mM Hepes, pH 7.5, 150 mM NaCl, 50 mM NaF, 1 mM activated Na_3VO_4 , 0.5 mM EDTA, 1 mM phenylmethylsulfonyl fluoride, 10 mM iodoacetamide, and $1 \mu\text{g}/\text{ml}$ protease inhibitor cocktail (Sigma-Aldrich). CD3 ζ was immunoprecipitated by incubation with anti-CD3 ζ agarose beads for 1 h. Reduced samples were resolved by SDS-PAGE and transferred onto PVDF membranes (Bio-Rad Laboratories). Membranes were blocked with 3% BSA in TBS and immunoblotted with biotinylated anti-pTyr-100 and streptavidin-HRP (Sigma-Aldrich), or anti-CD3 ζ -HRP. Blots were visualized with ECL Western blotting kit (PerkinElmer).

2D T cell kinetic measurements by micropipette adhesion frequency. Human RBCs isolated in accordance with the IRB at the Georgia Institute of Technology were coated with various concentrations of Biotin-X-NHS (EMD). The RBCs were washed, coated with $0.5 \text{ mg}/\text{ml}$ streptavidin (Thermo Fisher Scientific), washed again, and incubated with 1–2 μg of the indicated pMHC monomer. All incubations were performed at 4°C on a rotator. The site densities (molecules/ μm^2) of pMHC II monomers per RBC and TCRs per T cell were derived by staining with anti-MHC II and anti-TCR PE-labeled antibodies, respectively, and the MFI was normalized using PE QuantiBRITE beads (BD) as previously described (Huang et al., 2010). The details of the micropipette adhesion frequency assay are described in detail elsewhere (Huang et al., 2007, 2010). In brief, a pMHC-coated RBC and a T cell were placed on opposing micropipettes and brought into contact by micromanipulation for a controlled contact area (A_c) and time (t). The contact duration varied from 0.1 to 10 s and the contact area was kept constant for all experiments so it would not affect affinity comparisons. At the end of the contact period, the T cell was retracted and the occurrence of adhesion (i.e., TCR/pMHC ligation) was observed microscopically as elongation of the RBC membrane. Each T cell–RBC pair underwent 50 contact-retraction cycles to calculate an adhesion frequency (P_a) at a given contact time. Using the mean adhesion frequency at equilibrium, $P_a(\infty)$, the 2D affinity ($A_c K_a$) was calculated as:

$$A_c K_a = \ln \left[\ln \left[1 - P_a(\infty) / (m_r m_l) \right] \right],$$

where m_r and m_l reflect the receptor (TCR) and ligand (pMHC) densities, respectively. The 2D off-rate (k_{off}) was calculated by:

$$k_{\text{off}} = \frac{1}{t_{1/2}} \ln \left\{ 1 - \frac{\ln \left[1 - \frac{1}{2} P_a(\infty) \right]}{\ln \left[1 - P_a(\infty) \right]} \right\}^{-1},$$

where $t_{1/2}$ is the time to reach the half-maximal P_a at equilibrium. The 2D on-rate ($A_c K_{\text{on}}$) was calculated from $k_{\text{on}} = K_a \times k_{\text{off}}$.

Tetramer staining. Biotinylated MHC class II–peptide complexes were incubated with streptavidin-PE (Invitrogen) at a 4:1 molar ratio for 1 h at room temperature. T cells (0.5×10^6 per sample) were incubated with $20 \mu\text{g}/\text{ml}$ tetramer for 1 h at room temperature, and then stained with Alexa Fluor 488–labeled anti-CD4 on ice. Cells were washed and analyzed on a FACSCalibur (BD). Data were processed with FlowJo software (Tree Star).

Proliferation and cytokine assays. To determine proliferation, 50×10^3 T cells were co-cultured in a 1:1 ratio (5:1 T cell/B cell ratio for Hy.1B11) with irradiated EBV-transformed B cell lines that had been treated with $50 \mu\text{g}/\text{ml}$ mitomycin C for 30 min at 37°C . Hy.1B11 and 9009 cells were cultured in media supplemented with 10% human serum 5 d before proliferation assays because Hy.1B11 T cells proliferated to an antigen present in bovine serum. Cells were plated in $0.2 \text{ ml}/\text{well}$ of a 96-well round bottom plate in AIM-V media (Invitrogen) supplemented with 2 mM GlutaMAX-I. Peptides were tested over a wide concentration range (in triplicates) and proliferation was assessed by [^3H]-thymidine incorporation after 72 h of culture. Cytokine assays were set up in the same fashion and supernatants were harvested after 24 h to measure IL-2 production using cytometric beads (CBA human IL-2 Flex Set; BD) according to the manufacturer's instructions.

Modulation of surface receptor expression levels. T cells were mixed 1:1 with peptide-loaded B cells ($0.15 \mu\text{M}$ peptide), plated in a 96-well round bottom culture dish, briefly spun down, and incubated at 37°C . After the indicated time points, cells were thoroughly resuspended in prechilled PBS containing 2 mM EDTA, and stained with PE-anti-CD3, APC-anti-CD69, and Alexa Fluor 488-anti-CD4 antibodies in 5% FBS on ice for 30 min. Cells were washed and fixed with 2% formaldehyde for 20 min before analysis by flow cytometry on a FACSCalibur (BD).

Online supplemental material. Videos 1–4 show 90-min time-lapse videos of IS formation for HA:D7, Ob.1A12, Hy.1B11, and Agad303 T cell clones on lipid bilayers. Videos 5–7 show real-time Ca^{2+} mobilization in HA:D7, Ob.1A12, and Agad325 T cell clones upon interaction with peptide-pulsed B cells. Online supplemental material is available at <http://www.jem.org/cgi/content/full/jem.20111485/DC1>.

We thank David Haffler (Yale School of Medicine, CT) for helpful discussions, Mark M. Davis (Stanford University School of Medicine, CA) for the baculovirus clone expressing I-E* molecules, and Daniel M. Altmann (Imperial College, London, U.K.) for the transgenic mice expressing HLA-DR15 and Ob.1A12 TCR.

This work was supported by grants from the National Institutes of Health (P01 AI045757 to K.W. Wucherpfennig and M.L. Dustin) and by postdoctoral fellowships from the Cancer Research Institute (to D.A. Schubert and E. Gagnon), the Ernst-Schering Foundation (to D.A. Schubert), the Generalitat de Catalunya – AGAUR (to S. Gordo), and the National Multiple Sclerosis Society (to D.K. Sethi).

The authors declare no competing financial interests.

Submitted: 19 July 2011

Accepted: 9 January 2012

REFERENCES

- Anders, A.K., M.J. Call, M.S. Schulze, K.D. Fowler, D.A. Schubert, N.P. Seth, E.J. Sundberg, and K.W. Wucherpfennig. 2011. HLA-DM captures partially empty HLA-DR molecules for catalyzed removal of peptide. *Nat. Immunol.* 12:54–61. <http://dx.doi.org/10.1038/ni.1967>
- Anderson, A.C., L.B. Nicholson, K.L. Legge, V. Turchin, H. Zaghouani, and V.K. Kuchroo. 2000. High frequency of autoreactive myelin proteolipid protein-specific T cells in the periphery of naive mice: mechanisms of selection of the self-reactive repertoire. *J. Exp. Med.* 191:761–770. <http://dx.doi.org/10.1084/jem.191.5.761>
- Anderson, M.S., E.S. Venanzi, L. Klein, Z. Chen, S.P. Berzins, S.J. Turley, H. von Boehmer, R. Bronson, A. Dierich, C. Benoist, and D. Mathis. 2002. Projection of an immunological self shadow within the thymus by the aire protein. *Science*. 298:1395–1401. <http://dx.doi.org/10.1126/science.1075958>
- Barrett, J.C., D.G. Clayton, P. Concannon, B. Akolkar, J.D. Cooper, H.A. Erlich, C. Julier, G. Morahan, J. Nerup, C. Nierras, et al; Type 1 Diabetes Genetics Consortium. 2009. Genome-wide association study and meta-analysis find that over 40 loci affect risk of type 1 diabetes. *Nat. Genet.* 41:703–707. <http://dx.doi.org/10.1038/ng.381>
- Brennan, M., P.F. Davison, and H. Paulus. 1985. Preparation of bispecific antibodies by chemical recombination of monoclonal immunoglobulin G1 fragments. *Science*. 229:81–83. <http://dx.doi.org/10.1126/science.3925553>

- Campi, G., R. Varma, and M.L. Dustin. 2005. Actin and agonist MHC-peptide complex-dependent T cell receptor microclusters as scaffolds for signaling. *J. Exp. Med.* 202:1031–1036. <http://dx.doi.org/10.1084/jem.20051182>
- Cemerski, S., J. Das, J. Locasale, P. Arnold, E. Giuriso, M.A. Markiewicz, D. Fremont, P.M. Allen, A.K. Chakraborty, and A.S. Shaw. 2007. The stimulatory potency of T cell antigens is influenced by the formation of the immunological synapse. *Immunity*. 26:345–355. <http://dx.doi.org/10.1016/j.immuni.2007.01.013>
- Cemerski, S., J. Das, E. Giuriso, M.A. Markiewicz, P.M. Allen, A.K. Chakraborty, and A.S. Shaw. 2008. The balance between T cell receptor signaling and degradation at the center of the immunological synapse is determined by antigen quality. *Immunity*. 29:414–422. <http://dx.doi.org/10.1016/j.immuni.2008.06.014>
- Davis, S.J., and P.A. van der Merwe. 2006. The kinetic-segregation model: TCR triggering and beyond. *Nat. Immunol.* 7:803–809. <http://dx.doi.org/10.1038/ni1369>
- Day, C.L., N.P. Seth, M. Lucas, H. Appel, L. Gauthier, G.M. Lauer, G.K. Robbins, Z.M. Szczepiorkowski, D.R. Casson, R.T. Chung, et al. 2003. Ex vivo analysis of human memory CD4 T cells specific for hepatitis C virus using MHC class II tetramers. *J. Clin. Invest.* 112:831–842.
- Derbinski, J., A. Schulte, B. Kyewski, and L. Klein. 2001. Promiscuous gene expression in medullary thymic epithelial cells mirrors the peripheral self. *Nat. Immunol.* 2:1032–1039. <http://dx.doi.org/10.1038/ni723>
- Dustin, M.L. 2007. Cell adhesion molecules and actin cytoskeleton at immune synapses and kinapses. *Curr. Opin. Cell Biol.* 19:529–533. <http://dx.doi.org/10.1016/j.ccb.2007.08.003>
- Dustin, M.L., and D. Depoil. 2011. New insights into the T cell synapse from single molecule techniques. *Nat. Rev. Immunol.* 11:672–684. <http://dx.doi.org/10.1038/nri3066>
- Dustin, M.L., T. Starr, R. Varma, and V.K. Thomas. 2007. Supported planar bilayers for study of the immunological synapse. *Curr. Protoc. Immunol.* Chapter 18:18.13.
- Ellmerich, S., M. Mycko, K. Takacs, H. Waldner, F.N. Wahid, R.J. Boyton, R.H. King, P.A. Smith, S. Amor, A.H. Herlihy, et al. 2005. High incidence of spontaneous disease in an HLA-DR15 and TCR transgenic multiple sclerosis model. *J. Immunol.* 174:1938–1946.
- Feng, D., C.J. Bond, L.K. Ely, J. Maynard, and K.C. Garcia. 2007. Structural evidence for a germline-encoded T cell receptor-major histocompatibility complex interaction ‘codon’. *Nat. Immunol.* 8:975–983. <http://dx.doi.org/10.1038/ni1502>
- Fleire, S.J., and F.D. Batista. 2009. Studying cell-to-cell interactions: an easy method of tethering ligands on artificial membranes. *Methods Mol. Biol.* 462:145–154. http://dx.doi.org/10.1007/978-1-60327-115-8_9
- Friedman, R.S., P. Beemiller, C.M. Sorensen, J. Jacobelli, and M.F. Krummel. 2010. Real-time analysis of T cell receptors in naive cells in vitro and in vivo reveals flexibility in synapse and signaling dynamics. *J. Exp. Med.* 207:2733–2749. <http://dx.doi.org/10.1084/jem.20091201>
- Grakoui, A., S.K. Bromley, C. Sumen, M.M. Davis, A.S. Shaw, P.M. Allen, and M.L. Dustin. 1999. The immunological synapse: a molecular machine controlling T cell activation. *Science*. 285:221–227. <http://dx.doi.org/10.1126/science.285.5425.221>
- Gütgemann, I., A.M. Fahrner, J.D. Altman, M.M. Davis, and Y.H. Chien. 1998. Induction of rapid T cell activation and tolerance by systemic presentation of an orally administered antigen. *Immunity*. 8:667–673.
- Hafner, D.A., A. Compston, S. Sawcer, E.S. Lander, M.J. Daly, P.L. De Jager, P.I. de Bakker, S.B. Gabriel, D.B. Mirel, A.J. Ivinson, et al.; International Multiple Sclerosis Genetics Consortium. 2007. Risk alleles for multiple sclerosis identified by a genome-wide study. *N. Engl. J. Med.* 357:851–862. <http://dx.doi.org/10.1056/NEJMoa073493>
- Hahn, M., M.J. Nicholson, J. Pyrdol, and K.W. Wucherpfennig. 2005. Unconventional topology of self peptide-major histocompatibility complex binding by a human autoimmune T cell receptor. *Nat. Immunol.* 6:490–496. <http://dx.doi.org/10.1038/ni1187>
- Hailman, E., W.R. Burack, A.S. Shaw, M.L. Dustin, and P.M. Allen. 2002. Immature CD4(+)CD8(+) thymocytes form a multifocal immunological synapse with sustained tyrosine phosphorylation. *Immunity*. 16:839–848. [http://dx.doi.org/10.1016/S1074-7613\(02\)00326-6](http://dx.doi.org/10.1016/S1074-7613(02)00326-6)
- He, X.L., C. Radu, J. Sidney, A. Sette, E.S. Ward, and K.C. Garcia. 2002. Structural snapshot of aberrant antigen presentation linked to autoimmunity: the immunodominant epitope of MBP complexed with I-Au. *Immunity*. 17:83–94. [http://dx.doi.org/10.1016/S1074-7613\(02\)00340-0](http://dx.doi.org/10.1016/S1074-7613(02)00340-0)
- Huang, J., L.J. Edwards, B.D. Evavold, and C. Zhu. 2007. Kinetics of MHC-CD8 interaction at the T cell membrane. *J. Immunol.* 179:7653–7662.
- Huang, J., V.I. Zarnitsyna, B. Liu, L.J. Edwards, N. Jiang, B.D. Evavold, and C. Zhu. 2010. The kinetics of two-dimensional TCR and pMHC interactions determine T-cell responsiveness. *Nature*. 464:932–936. <http://dx.doi.org/10.1038/nature08944>
- Huppa, J.B., M. Axmann, M.A. Mörtelmaier, B.F. Lillemeier, E.W. Newell, M. Brameshuber, L.O. Klein, G.J. Schütz, and M.M. Davis. 2010. TCR-peptide-MHC interactions in situ show accelerated kinetics and increased affinity. *Nature*. 463:963–967. <http://dx.doi.org/10.1038/nature08746>
- Jacobelli, J., S.A. Chmura, D.B. Buxton, M.M. Davis, and M.F. Krummel. 2004. A single class II myosin modulates T cell motility and stopping, but not synapse formation. *Nat. Immunol.* 5:531–538. <http://dx.doi.org/10.1038/ni1065>
- Johnson, K.G., S.K. Bromley, M.L. Dustin, and M.L. Thomas. 2000. A supramolecular basis for CD45 tyrosine phosphatase regulation in sustained T cell activation. *Proc. Natl. Acad. Sci. USA*. 97:10138–10143. <http://dx.doi.org/10.1073/pnas.97.18.10138>
- Kaizuka, Y., A.D. Douglass, R. Varma, M.L. Dustin, and R.D. Vale. 2007. Mechanisms for segregating T cell receptor and adhesion molecules during immunological synapse formation in Jurkat T cells. *Proc. Natl. Acad. Sci. USA*. 104:20296–20301. <http://dx.doi.org/10.1073/pnas.0710258105>
- Kersh, E.N., A.S. Shaw, and P.M. Allen. 1998. Fidelity of T cell activation through multistep T cell receptor zeta phosphorylation. *Science*. 281:572–575. <http://dx.doi.org/10.1126/science.281.5376.572>
- Klein, L., M. Klugmann, K.A. Nave, V.K. Tuohy, and B. Kyewski. 2000. Shaping of the autoreactive T-cell repertoire by a splice variant of self protein expressed in thymic epithelial cells. *Nat. Med.* 6:56–61. <http://dx.doi.org/10.1038/71540>
- Lee, K.H., A.D. Holdorf, M.L. Dustin, A.C. Chan, P.M. Allen, and A.S. Shaw. 2002. T cell receptor signaling precedes immunological synapse formation. *Science*. 295:1539–1542. <http://dx.doi.org/10.1126/science.1067710>
- Li, Y., Y. Huang, J. Lue, J.A. Quandt, R. Martin, and R.A. Mariuzza. 2005. Structure of a human autoimmune TCR bound to a myelin basic protein self-peptide and a multiple sclerosis-associated MHC class II molecule. *EMBO J.* 24:2968–2979. <http://dx.doi.org/10.1038/sj.emboj.7600771>
- Madsen, L.S., E.C. Andersson, L. Jansson, M. Krogsgaard, C.B. Andersen, J. Engberg, J.L. Strominger, A. Svejgaard, J.P. Hjorth, R. Holmdahl, et al. 1999. A humanized model for multiple sclerosis using HLA-DR2 and a human T-cell receptor. *Nat. Genet.* 23:343–347. <http://dx.doi.org/10.1038/15525>
- Maynard, J., K. Petersson, D.H. Wilson, E.J. Adams, S.E. Blondelle, M.J. Boulanger, D.B. Wilson, and K.C. Garcia. 2005. Structure of an autoimmune T cell receptor complexed with class II peptide-MHC: insights into MHC bias and antigen specificity. *Immunity*. 22:81–92.
- Mempel, T.R., S.E. Henrickson, and U.H. Von Andrian. 2004. T-cell priming by dendritic cells in lymph nodes occurs in three distinct phases. *Nature*. 427:154–159. <http://dx.doi.org/10.1038/nature02238>
- Monks, C.R., B.A. Freiberg, H. Kupfer, N. Sciaky, and A. Kupfer. 1998. Three-dimensional segregation of supramolecular activation clusters in T cells. *Nature*. 395:82–86. <http://dx.doi.org/10.1038/25764>
- Nepom, G.T., J.D. Lippolis, F.M. White, S. Masewicz, J.A. Marto, A. Herman, C.J. Luckey, B. Falk, J. Shabanowitz, D.F. Hunt, et al. 2001. Identification and modulation of a naturally processed T cell epitope from the diabetes-associated autoantigen human glutamic acid decarboxylase 65 (hGAD65). *Proc. Natl. Acad. Sci. USA*. 98:1763–1768. <http://dx.doi.org/10.1073/pnas.98.4.1763>
- Nicholson, M.J., B. Moradi, N.P. Seth, X. Xing, G.D. Cuny, R.L. Stein, and K.W. Wucherpfennig. 2006. Small molecules that enhance the catalytic efficiency of HLA-DM. *J. Immunol.* 176:4208–4220.

- Pribyl, T.M., C. Campagnoni, K. Kampf, V.W. Handley, and A.T. Campagnoni. 1996. The major myelin protein genes are expressed in the human thymus. *J. Neurosci. Res.* 45:812–819. [http://dx.doi.org/10.1002/\(SICI\)1097-4547\(19960915\)45:6<812::AID-JNR18>3.0.CO;2-X](http://dx.doi.org/10.1002/(SICI)1097-4547(19960915)45:6<812::AID-JNR18>3.0.CO;2-X)
- Pugliese, A., M. Zeller, A. Fernandez Jr., L.J. Zalcberg, R.J. Bartlett, C. Ricordi, M. Pietropaolo, G.S. Eisenbarth, S.T. Bennett, and D.D. Patel. 1997. The insulin gene is transcribed in the human thymus and transcription levels correlated with allelic variation at the INS VNTR-IDD2 susceptibility locus for type 1 diabetes. *Nat. Genet.* 15:293–297. <http://dx.doi.org/10.1038/ng0397-293>
- Qian, D., and A. Weiss. 1997. T cell antigen receptor signal transduction. *Curr. Opin. Cell Biol.* 9:205–212. [http://dx.doi.org/10.1016/S0955-0674\(97\)80064-6](http://dx.doi.org/10.1016/S0955-0674(97)80064-6)
- Reijonen, H., R. Mallone, A.K. Heninger, E.M. Laughlin, S.A. Kochik, B. Falk, W.W. Kwok, C. Greenbaum, and G.T. Nepom. 2004. GAD65-specific CD4+ T-cells with high antigen avidity are prevalent in peripheral blood of patients with type 1 diabetes. *Diabetes.* 53:1987–1994. <http://dx.doi.org/10.2337/diabetes.53.8.1987>
- Richie, L.I., P.J. Ebert, L.C. Wu, M.F. Krummel, J.J. Owen, and M.M. Davis. 2002. Imaging synapse formation during thymocyte selection: inability of CD3zeta to form a stable central accumulation during negative selection. *Immunity.* 16:595–606. [http://dx.doi.org/10.1016/S1074-7613\(02\)00299-6](http://dx.doi.org/10.1016/S1074-7613(02)00299-6)
- Roucard, C., F. Garban, N.A. Mooney, D.J. Charron, and M.L. Ericson. 1996. Conformation of human leukocyte antigen class II molecules. Evidence for superdimers and empty molecules on human antigen presenting cells. *J. Biol. Chem.* 271:13993–14000. <http://dx.doi.org/10.1074/jbc.271.24.13993>
- Sabatino, J.J. Jr., J. Huang, C. Zhu, and B.D. Evavold. 2011. High prevalence of low affinity peptide-MHC II tetramer-negative effectors during polyclonal CD4+ T cell responses. *J. Exp. Med.* 208:81–90. <http://dx.doi.org/10.1084/jem.20101574>
- Samstag, Y., S.M. Eibert, M. Klemke, and G.H. Wabnitz. 2003. Actin cytoskeletal dynamics in T lymphocyte activation and migration. *J. Leukoc. Biol.* 73:30–48. <http://dx.doi.org/10.1189/jlb.0602272>
- Seder, R.A., W.E. Paul, M.M. Davis, and B. Fazekas de St Groth. 1992. The presence of interleukin 4 during in vitro priming determines the lymphokine-producing potential of CD4+ T cells from T cell receptor transgenic mice. *J. Exp. Med.* 176:1091–1098. <http://dx.doi.org/10.1084/jem.176.4.1091>
- Sethi, D.K., D.A. Schubert, A.K. Anders, A. Heroux, D.A. Bonsor, C.P. Thomas, E.J. Sundberg, J. Pyrdol, and K.W. Wucherpfennig. 2011. A highly tilted binding mode by a self-reactive T cell receptor results in altered engagement of peptide and MHC. *J. Exp. Med.* 208:91–102. <http://dx.doi.org/10.1084/jem.20100725>
- Sims, T.N., T.J. Soos, H.S. Xenias, B. Dubin-Thaler, J.M. Hofman, J.C. Waite, T.O. Cameron, V.K. Thomas, R. Varma, C.H. Wiggins, et al. 2007. Opposing effects of PKCtheta and WASp on symmetry breaking and relocation of the immunological synapse. *Cell.* 129:773–785. <http://dx.doi.org/10.1016/j.cell.2007.03.037>
- Stanley, P. 1989. Chinese hamster ovary cell mutants with multiple glycosylation defects for production of glycoproteins with minimal carbohydrate heterogeneity. *Mol. Cell. Biol.* 9:377–383.
- Sumen, C., M.L. Dustin, and M.M. Davis. 2004. T cell receptor antagonism interferes with MHC clustering and integrin patterning during immunological synapse formation. *J. Cell Biol.* 166:579–590. <http://dx.doi.org/10.1083/jcb.200404059>
- Todd, J.A., J.I. Bell, and H.O. McDevitt. 1987. HLA-DQ beta gene contributes to susceptibility and resistance to insulin-dependent diabetes mellitus. *Nature.* 329:599–604. <http://dx.doi.org/10.1038/329599a0>
- Tseng, S.Y., J.C. Waite, M. Liu, S. Vardhana, and M.L. Dustin. 2008. T cell-dendritic cell immunological synapses contain TCR-dependent CD28-CD80 clusters that recruit protein kinase C theta. *J. Immunol.* 181:4852–4863.
- Valitutti, S., M. Dessing, K. Aktories, H. Gallati, and A. Lanzavecchia. 1995a. Sustained signaling leading to T cell activation results from prolonged T cell receptor occupancy. Role of T cell actin cytoskeleton. *J. Exp. Med.* 181:577–584. <http://dx.doi.org/10.1084/jem.181.2.577>
- Valitutti, S., S. Müller, M. Cella, E. Padovan, and A. Lanzavecchia. 1995b. Serial triggering of many T-cell receptors by a few peptide-MHC complexes. *Nature.* 375:148–151. <http://dx.doi.org/10.1038/375148a0>
- Vardhana, S., K. Choudhuri, R. Varma, and M.L. Dustin. 2010. Essential role of ubiquitin and TSG101 protein in formation and function of the central supramolecular activation cluster. *Immunity.* 32:531–540. <http://dx.doi.org/10.1016/j.immuni.2010.04.005>
- Varma, R., G. Campi, T. Yokosuka, T. Saito, and M.L. Dustin. 2006. T cell receptor-proximal signals are sustained in peripheral microclusters and terminated in the central supramolecular activation cluster. *Immunity.* 25:117–127. <http://dx.doi.org/10.1016/j.immuni.2006.04.010>
- Wucherpfennig, K.W., and D. Sethi. 2011. T cell receptor recognition of self and foreign antigens in the induction of autoimmunity. *Semin. Immunol.* 23:84–91. <http://dx.doi.org/10.1016/j.smim.2011.01.007>
- Wucherpfennig, K.W., A. Sette, S. Southwood, C. Oseroff, M. Matsui, J.L. Strominger, and D.A. Hafler. 1994. Structural requirements for binding of an immunodominant myelin basic protein peptide to DR2 isotypes and for its recognition by human T cell clones. *J. Exp. Med.* 179:279–290. <http://dx.doi.org/10.1084/jem.179.1.279>
- Yin, Y., Y. Li, M.C. Kerzic, R. Martin, and R.A. Mariuzza. 2011. Structure of a TCR with high affinity for self-antigen reveals basis for escape from negative selection. *EMBO J.* 30:1137–1148. <http://dx.doi.org/10.1038/emboj.2011.21>
- Yokosuka, T., K. Sakata-Sogawa, W. Kobayashi, M. Hiroshima, A. Hashimoto-Tane, M. Tokunaga, M.L. Dustin, and T. Saito. 2005. Newly generated T cell receptor microclusters initiate and sustain T cell activation by recruitment of Zap70 and SLP-76. *Nat. Immunol.* 6:1253–1262. <http://dx.doi.org/10.1038/ni1272>
- Yokosuka, T., W. Kobayashi, K. Sakata-Sogawa, M. Takamatsu, A. Hashimoto-Tane, M.L. Dustin, M. Tokunaga, and T. Saito. 2008. Spatiotemporal regulation of T cell costimulation by TCR-CD28 microclusters and protein kinase C theta translocation. *Immunity.* 29:589–601. <http://dx.doi.org/10.1016/j.immuni.2008.08.011>